AFRL-MN-EG-TR-2007-7013 DTIC/STINFO COPY

POSSIBLE GRAVITATIONAL ANOMALIES IN QUANTUM MATERIALS
Phase II: Experiment Assembly, Qualification and Test Results

M. Tajmar

Austrian Research Centers Seibersdorf Research GmbH
A-2444 Seibersdorf, Austria

Award No. FA8655-03-1-3075

February 2007

FINAL REPORT FOR PERIOD March 2004 – September 2005

AIR FORCE RESEARCH LABORATORY, MUNITIONS DIRECTORATE
Air Force Materiel Command ■ United States Air Force ■ Eglin Air Force Base

NOTICE AND SIGNATURE PAGE

Using Government drawings, specifications, or other data included in this document for any purpose other than Government procurement does not in any way obligate the U.S. Government. The fact that the Government formulated or supplied the drawings, specifications, or other data does not license the holder or any other person or corporation; or convey any rights or permission to manufacture, use, or sell any patented invention that may relate to them.

This report was cleared for public release by the Air Armament Center Public Affairs Office and is available to the general public, including foreign nationals. Copies may be obtained from the Defense Technical Information Center (DTIC) (http://www.dtic.mil).

AFRL-MN-EG-TR-2007-7013 HAS BEEN REVIEWED AND IS APPROVED FOR PUBLICATION IN ACCORDANCE WITH ASSIGNED DISTRIBUTION STATEMENT.

FOR THE DIRECTOR:

// original signed //	*// original signed //*	*// original signed //*
DANNY R. HAYLES	KIRK E. HERZOG	DONALD M. LITTRELL
Technical Director	Technical Advisor	Program Manager
Ordnance Division	Damage Mechanisms Branch	Damage Mechanisms Branch

This report is published in the interest of scientific and technical information exchange, and its publication does not constitute the Government's approval or disapproval of its ideas or findings.

REPORT DOCUMENTATION PAGE

Form Approved
OMB No. 0704-0188

1. REPORT DATE *(DD-MM-YYYY)*	**2. REPORT TYPE**	**3. DATES COVERED** *(From - To)*
February 2007	Final	March 2004 – September 2005

4. TITLE AND SUBTITLE

POSSIBLE GRAVITATIONAL ANOMALIES IN QUANTUM MATERIALS
Phase II: Experiment Assembly, Qualification and Test Results

5a. CONTRACT NUMBER

5b. GRANT NUMBER
FA8655-03-1-3075

5c. PROGRAM ELEMENT NUMBER
62602F

6. AUTHOR(S)
M. Tajmar

Austrian Research Centers Seibersdorf Research GmbH
A-2444 Seibersdorf, Austria

5d. PROJECT NUMBER
2502

5e. TASK NUMBER
99

5f. WORK UNIT NUMBER
14

7. PERFORMING ORGANIZATION NAME(S) AND ADDRESS(ES)

Austrian Research Centers Seibersdorf Research GmbH
A-2444 Seibersdorf, Austria

8. PERFORMING ORGANIZATION REPORT NUMBER

9. SPONSORING / MONITORING AGENCY NAME(S) AND ADDRESS(ES)
Air Force Research Laboratory
Munitions Directorate, AFRL/MNMW
101 W. Eglin Blvd., Ste. 135
Eglin AFB FL 32542-6810

10. SPONSOR/MONITOR'S ACRONYM(S)
AFRL-MN-EG

11. SPONSOR/MONITOR'S REPORT NUMBER(S)
AFRL-MN-EG-TR-2007-7013

12. DISTRIBUTION / AVAILABILITY STATEMENT
DISTRIBUTION A: Approved for public release; distribution unlimited. AAC/PA Approval and Clearance # 01-12-07-016, dated 12 January 2007.

13. SUPPLEMENTARY NOTES

14. ABSTRACT: The author recently published a paper, suggesting for the first time that a reported disagreement between experimental measurements and theoretical predictions for the magnetic field in rotating superconductors might arise from an anomalous high-order gravitomagnetic contribution (also known as frame dragging or Lense-Thirring effect). In normal matter, the ratio between electromagnetic and gravitational fields is given by the difference in the respective permeabilities. However, magnetic fields generated as a consequence of the quantization of the canonical momentum in a superconductor do not depend on the permeability. Hence, there is the possibility that the ratio between those two fields might be different in a quantum material. Latest theoretical work links the generation of those non-classical gravitomagnetic fields to the ratio between the Cooper-pair mass and the bulk density of the superconductor.

This report summarizes the work carried out in Phase II – the assembly of the experiment, qualification to make sure that the required sensitivity can be met, and finally the report on the test results using BSCCO and YBCO superconductors as well as Niobium as a dummy at liquid nitrogen temperatures. The measurements show that the resolution level is low enough to test the original conditions defined in Phase I (derived from Tate's Cooper-pair measurements), however, the resolution is about one order of magnitude above the theoretical predictions for high-temperature superconductors. No gravitational anomalies were found for BSCCO and YBCO down to the facility resolution level. Hence, gravitational fields based on Tate's measurement have not been found with high-temperature superconductors. However, the results do not rule out such gravitational anomalies at their theoretically predicted lower values or anomalies using Tate's original setup (Niobium superconductor and liquid helium temperatures).

15. SUBJECT TERMS
gravitational anomaly, superconductor, frame dragging, Lense-Thirring effect, quantum material, magnetic field, gravity, gravitomagnetic field, Cooper pair

16. SECURITY CLASSIFICATION OF:			**17. LIMITATION OF ABSTRACT**	**18. NUMBER OF PAGES**	**19a. NAME OF RESPONSIBLE PERSON**
a. REPORT	**b. ABSTRACT**	**c. THIS PAGE**			Donald M. Littrell
UNCLASSIFIED	UNCLASSIFIED	UNCLASSIFIED	SAR	56	**19b. TELEPHONE NUMBER** *(include area code)*

PREFACE

Dr. Martin Tajmar of the Austrian Research Centers (ARC) Seibersdorf presented a briefing on this subject at the Air Force Research Laboratory, Munitions Directorate (AFRL/MN), Eglin Air Force Base, Florida in the Fall of 2002 under the Window on Science (WOS) program managed by the European Office of Aerospace Research and Development (EOARD, Det. 1, AFOSR). ARC Seibersdorf submitted a formal proposal through AFOSR Broad Agency Announcement (BAA) 2003-1, and AFRL/MN sent Military Departmental Purchase Requests (MIPRs) to EOARD in August 2003 to fund Phase I of this effort and in February 2004 to fund Phase II. EOARD performed the contracting functions and AFRL/MN performed the programmatic and technical management functions.

This report documents the second phase of this project. The first phase is documented in AFRL/MN technical report AFRL-MN-EG-TR-2007-7012, “Possible Gravitational Anomalies in Quantum Materials, Phase I: Experiment Definition and Design,” by M. Tajmar and K. Hense, February 2007.

POSSIBLE GRAVITATIONAL ANOMALIES IN QUANTUM MATERIALS

Phase II: Experiment Assembly, Qualification and Test Results

Award No. FA8655-03-1-3075

Date: 15. 09. 2005

Prepared by: M. Tajmar, ARC Seibersdorf research

ABSTRACT

The author recently published a paper, suggesting for the first time that a reported disagreement between experimental measurements and theoretical predictions for the magnetic field in rotating superconductors might arise from an anomalous high-order gravitomagnetic contribution (also known as frame dragging or Lense-Thirring effect). In normal matter, the ratio between electromagnetic and gravitational fields is given by the difference in the respective permeabilities. However, magnetic fields generated as a consequence of the quantization of the canonical momentum in a superconductor do not depend on the permeability. Hence, there is the possibility that the ratio between those two fields might be different in a quantum material. Latest theoretical work links the generation of those non-classical gravitomagnetic fields to the ratio between the Cooper-pair mass and the bulk density of the superconductor.

This report summarizes the work carried out in Phase II – the assembly of the experiment, qualification to make sure that the required sensitivity can be met, and finally the report on the test results using BSCCO and YBCO superconductors as well as Niobium as a dummy at liquid nitrogen temperatures. The measurements show that the resolution level is low enough to test the original conditions defined in Phase I (derived from Tate's Cooper-pair measurements), however, the resolution is about one order of magnitude above the theoretical predictions for high-temperature superconductors. No gravitational anomalies were found for BSCCO and YBCO down to the facility resolution level. Hence, gravitational fields based on Tate's measurement have not been found with high-temperature superconductors. However, the results do not rule out such gravitational anomalies at their theoretically predicted lower values or anomalies using Tate's original setup (Niobium superconductor and liquid helium temperatures).

TABLE OF CONTENT

1 THEORETICAL PREDICTIONS

1.1 Large Gravitomagnetic Fields based on Tate's Results

The experiment is designed to test the hypothesis, that large gravitomagnetic fields are responsible for the Cooper-mass anomaly measured by Tate et al (Tate et al, 1989, 1990). In a rotating superconductor (see Figure 1.1-1), the integral of the canonical momentum is quantized. In the case of a superconductive ring, if the ring's thickness is larger than the London penetration depth (usually in the order of 100 nm), then the integral can be set to zero,

$$\oint \vec{p}_S \cdot d\vec{l} = \oint \left(m\vec{v}_S + e\vec{A} \right) \cdot d\vec{l} = 0 \,, \tag{1}$$

where *m* and *e* are the mass and charge of the Cooper-pair, $\vec{A}$ the magnetic vector potential, and $\vec{v}_s$ the speed of the Cooper-pairs.

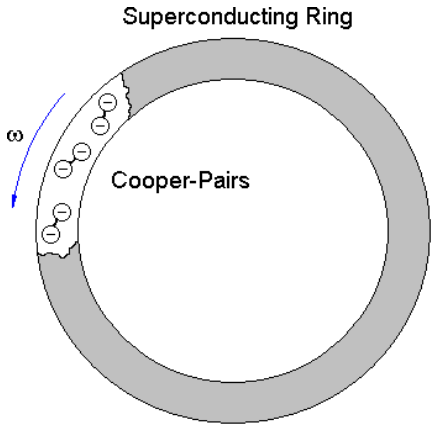

Figure 1.1-1 Rotating Superconductor

If a superconductor that was cooled down at rest (v_S=0) is now set into rotation (i.e. , $v_S \neq 0$), then it has to build up a magnetic field to still fulfill Equ. (1). One can easily transform Equ. (1) into

$$\vec{B} = -\frac{2m}{e}\vec{\omega} \,. \tag{2}$$

This is called the London moment. It is remarkable, because a magnetic field is generated without the permeability μ_0, which appears in all classical equations involving the magnetic fields.

By accurately measuring the magnetic field of a rotating superconductor (e.g. by using a SQUID) and the angular velocity ω, one can calculate the mass of the Cooper-pair (as the charge is always two times the elementary charge). This has been done for a number of superconductors (Tajmar et al, 2005 and references therein), the most important result was that the Cooper-pair mass is very close to two times the electron mass independent on the material used. Tate et al performed the most accurate

experiment up to now (Tate et al, 1989, 1990) revealing that the Cooper-pair mass is $m^*/2m_e$ = 1.000084(21) actually a little bit larger than two times the electron mass. This is even more a surprise as quantum theory including relativistic corrections expects the Cooper-pair mass to be a little bit smaller than two times the electron mass $m^*/2m_e$ = 0.999992. The difference between experiment and theory is more than 4 sigma! This anomaly was discussed in the literature without any apparent solution (Tajmar et al, 2005 and references therein). It is even more striking that such a mass increase is simply impossible from a thermodynamic point of view.

Therefore, something must be wrong – or putting in better words – not complete. Therefore Tajmar et al recently suggested (Tajmar et al, 2003) that Equ. (1) must be replaced by the full canonical momentum equation. This is not new and was first noted by DeWitt in the 1960s (DeWitt, 1966). The full canonical momentum in Equ. (1) leads to

$$\oint \vec{p}_s \cdot d\vec{l} = \oint \left(m\vec{v}_s + e\vec{A} + m\vec{A}_g \right) \cdot d\vec{l} = 0 \ , \tag{3}$$

where $\vec{A}_g$ is the gravitomagnetic vector potential. Applying it to our case of a rotating superconductor, we get

$$\vec{B} = -\frac{2m}{e} \cdot \vec{\omega} - \frac{m}{e} \cdot \vec{B}_g \ . \tag{4}$$

Comparing with Equ. (2), this shows that a rotating superconductor is generating a gravitomagnetic field in addition to a magnetic field. Using Tate's experimental values and the theoretical predictions (Tajmar et al, 2005), we get the gravitomagnetic field that is necessary to correct Tate's result and to comply with quantum theory

$$\vec{B} = 2\vec{\omega}\left(\frac{\Delta m}{m} \right) = 1.84 \times 10^{-4} \vec{\omega} \, , \tag{5}$$

where Δm is the difference between experimental and theoretical Cooper-pair mass. If Tate's result is correct and quantum theory holds, then a rotating superconductor can indeed produce a gravitomagnetic field which is many orders of magnitude above the non-coherent matter result.

It is important to note that Equ. (5) was derived for Tate's setup, i.e. using a 40 nm thick Niobium ring rotating at a maximum frequency of 5 Hz at a temperature of 6 K. How will Δm change if we use a material different than Niobium? The Phase I design of this experiment was centered around a high-temperature superconductor made out of BSCCO tested together with liquid nitrogen – for simplicity and cost reasons. Can we still expect the same gravitomagnetic field in this experiment as the one derived from Tate's measurement?

1.2 Gravitomagnetic Fields Depending on Superconductor Material

Only very recent theoretical progress enables us to predict the gravitomagnetic field generated by different superconductor materials.

In modern Quantum Field Theory (QFT) superconductivity is explained in the following way: As a superconductor is passing its critical temperature, gauge symmetry is broken. This causes the photon to aquire mass via the Higgs mechanism (Ryder, 2003). The London penetration depth that we observe is then just the wavelength of the massive photon ($\lambda_L=\lambda_{Photon}$). One consequence of a massive photon is that the Maxwell equations transform into the Proca equations with two additional terms,

$$\begin{aligned} div\,\vec{E} &= \frac{\rho}{\varepsilon_0} - \left(\frac{m_{Photon}c}{\hbar}\right)^2 \cdot \varphi \\ div\,\vec{B} &= 0 \\ rot\,\vec{E} &= -\frac{\partial \vec{B}}{\partial t} \\ rot\,\vec{B} &= \mu_0 \rho \vec{v} + \frac{1}{c^2}\frac{\partial \vec{E}}{\partial t} - \left(\frac{m_{Photon}c}{\hbar}\right)^2 \cdot \vec{A} \end{aligned} \qquad (6)$$

The author has recently shown (de Matos et al, 2005) that by taking the rotational of the 4th equation and solving the differential equation, the photon mass reveals the two basic features of superconductivity: exponential shielding of electromagnetic fields (Meissner-Ochsenfeld effect) and the generation of a magnetic field by rotation (London moment with $\lambda_L=\lambda_{Photon}$),

$$B = B_0 \cdot e^{-\frac{x}{\lambda_{Photon}}} - 2\omega\frac{m}{e}\left(\frac{\lambda_{Photon}}{\lambda_L}\right)^2 . \qquad (7)$$

In a typical superconductor, the photon mass is then about 1/1000 of the electron mass. We see that the mass of the photon is responsible for the London moment. If the photon is so massive, why shall the graviton in a superconductor not be massive as well – leading to a gravitomagnetic London moment that we need to match Tate's Cooper-pair mass anomaly?

The Proca equations can be also expressed for gravitational fields modifying the Einstein-Maxwell equations used in the weak field approximation. Following the same arguments as above, we get,

$$B_g = B_{g0} \cdot e^{-\frac{x}{\lambda_g}} - 2\omega\left(\frac{\lambda_g}{\lambda_{Lg}}\right)^2 , \qquad (8)$$

where $\lambda_g = \frac{\hbar}{m_g c}$ is the graviton Compton wavelength, and the second term in Equ. (10) can be interpreted as a gravitomagnetic London moment, just as we need to match Tate's Cooper-pair anomaly (compare with Equ. 5!). The gravitomagnetic penetration depth λ_{Lg} is defined as (de Matos, 2004)

$$\lambda_{Lg} = i\sqrt{\frac{1}{\mu_{0g} n_s m}} \ , \tag{9}$$

where n_S is the Cooper-pair density. Both the penetration depth as well as the graviton wavelength is a complex number, as required by the positive cosmological constant measured in our universe (Novello et al, 2003). Using Tate's result, we can compute the value of the graviton mass inside a Niobium superconductor as

$$m_g = i \cdot \sqrt{\frac{\mu_{0g} n_s m^2 \hbar^2}{c^2 \Delta m}} = i \cdot 4.61 \times 10^{-55} \ kg \ . \tag{10}$$

This is "only" 14 orders of magnitude above its accepted free-space value from the cosmological constant measurement of $i.10^{-69}$ kg (De Matos et al, 2005), but it is still a small number. In a recent assessment, Modanese (Modanese, 2003) calculated the cosmological constant inside a superconductor taking into account the contribution of the Ginzburg-Landau wave function ψ_{GL} to the Lagrangian. He found that in the case of a Pb superconductor, the cosmological constant should be on the order of 10^{-39} m^{-2}. That would lead to a complex graviton mass of $i.10^{-62}$ kg, coming closer to our estimate of $i.10^{-55}$ kg in a Nb superconductor. By comparing Equs. (5) and (8), we find that

$$\frac{\Delta m}{m} = \left(\frac{\lambda_g}{\lambda_{Lg}} \right)^2 \ . \tag{11}$$

Hence, the delta of mass measured by Tate is just an expression of the ratio between the graviton wavelength and its penetration depth inside a superconductor.

In our very last theoretical assessment (Tajmar et al, to be published), we were able to further express the graviton wavelength inside the superconductor and express Equ (11) by

$$\frac{\Delta m}{m} = \frac{\rho_s}{\rho_{bulk}} \ , \tag{12}$$

where ρ_S is the Cooper-pair mass density and ρ_{bulk} the bulk density of the superconductor. The following table compares the results expected from Tate's setup to the conditions of high-temperature superconductors and liquid nitrogen as used in our experimental setup.

Material	Temperature [K]	Bulk Density [kg.m^{-3}]	Cooper-Pair Mass Density [kg.m^{-3}]	$\Delta m / m$
Niobium	6	8570	2.82×10^{-2}	3.29×10^{-6}
YBCO	77	6133	1.02×10^{-3}	1.67×10^{-7}
BSCCO (2212)	77	5400	3.78×10^{-4}	7.01×10^{-8}

Table 1 Expected Theoretical $\Delta m/m$ for Different Materials

We see that the theory ($\Delta m/m$=3.29x10^{-6}) already comes quite close, within a factor 28, to our derived value from Tate's experiment ($\Delta m/m$=9.2x10^{-5}) in case of Niobium at 6 K. The Δm is the difference between the theoretically expected and measured Cooper-pair mass, so additional theoretical corrections factors, already proposed by a number of papers (e.g. Capelle et al, 1999), might close the gap to our theoretical prediction.

1.3 Coupling Factor Expected in Experiment

The experiment can not measure the gravitomagnetic field predicted for rotating superconductors directly, but the induced gravitational field due to acceleration of the ring.

Using the gravitational induction law,

$$rot\ \vec{g} = -\frac{\partial \vec{B}_g}{\partial t} \ , \tag{13}$$

and Equ. (5), we can express the gravitational field measured at the radial distance r (if r < superconductor ring radius) by expanding Equ. (13),

$$\iint rot\ \vec{g} \cdot d\vec{A} = \oint \vec{g} \cdot d\vec{l} = -\iint 2\dot{\omega} \frac{\Delta m}{m} \cdot d\vec{A} \ , \tag{14}$$

and finally get for the one-dimenaional case

$$g = -\dot{\omega} r \frac{\Delta m}{m} \ . \tag{15}$$

For the experiment it is useful to define a coupling factor of the induced gravitational field versus the applied acceleration. For field units in terms of the standard Earth's gravitational acceleration (9.81m.s^{-2}), we get

$$\frac{g}{\dot{\omega}} = -\frac{r}{9.81} \frac{\Delta m}{m} \ . \tag{16}$$

The gravitational field, following the vectorial equations, should point in the opposite direction of the applied angular acceleration (tangential). The following table summarizes the predicted coupling factors for the In-Ring Sensors (r=4 cm) based on Tate's measurement and our theory.

Material	**Condition**	Temperature [K]	Predicted Angular Acceleration Coupling Factor [$s^2.rad^{-1}$]
Niobium	From Tate's Experiment	6	-3.7×10^{-7}
Niobium	From Theory	6	-1.2×10^{-8}
YBCO	From Theory	77	-6.1×10^{-10}
BSCCO (2212)	From Theory	77	-2.6×10^{-10}

Table 2 Expected Coupling Ratios for Different Materials

This shows that the coupling factor to be investigated by the experiment with high-temperature superconductors can be 2-3 orders of magnitude below the one derived from Tate's measurement, which was the basis for the design. Still, even the reduced coupling factors would lead to gravitational fields 20 orders of magnitude above classical values and are therefore very interesting for technological applications.

2 EXPERIMENT ASSEMBLY

2.1 Introduction

The experimental facility was initially manufactured, assembled and tested according to the original design plan of Phase I. However, extensive testing made the following two major changes necessary:

– Replacement of the Silicon Designs 1221 accelerometers with AppliedMEMS SF1500S accelerometers. The new accelerometers have a higher resolution (see Figure 2.1-1) and are less sensitive to magnetic fields that are coming from the electric motor (components of accelerometers are made out of non-magnetic components).

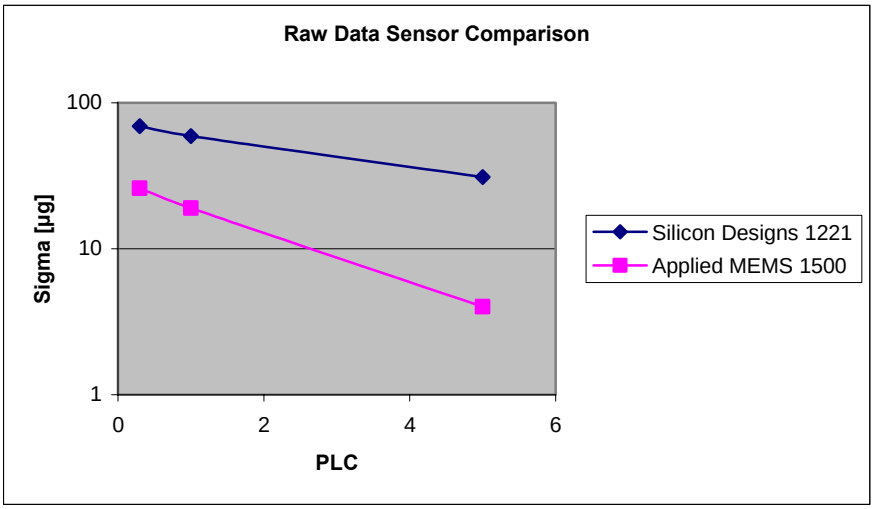

Figure 2.1-1 Sensor Noise Comparison for different Power Line Cycles (1 PLC corresponds to 20 ms)

– The damping system for the sensor-vacuum chamber had to be replaced by a fixed structure, mounted on the ground and roof, in order to efficiently stop the transmission of noise due to the rotation of the superconducting ring to the sensors. With the damping system, a noise level on the sensors of +/- 2 mg was observed during full rotation, which is at least one order of magnitude larger than the predicted effect (derived from Tate's experiment at maximum angular acceleration). In the fixed configuration, no effect due to the rotation of the superconductor could be seen any more and a noise level of about 20 µg was obtained at a sampling frequency of 10 Hz.

The following sections show step-by-step how the experimental facility was assembled.

2.2 Sensor-Vacuum Chamber

Three AppliedMEMS 1500S accelerometers (X-, Y, and Z-direction) were mounted on the three measurement positions (9 in total):

- above the superconductor (2.5 cm at a radial distance of 7.5 cm),
- inside the superconductor (at a radial distance of 4 cm),
- on reference position (20.5 cm above superconductor at a radial distance of 4 cm).

Next to each accelerometer, a Kapton heater foil was mounted for maintaining a temperature of 25°C at each sensor. Moreover, each measurement position (above ring, inner ring, reference) was equipped with a PT-100 element for temperature measurement. Figure 2.2-1 shows one accelerometer and a heater on the structure.

In addition to the accelerometers, high-resolution fluxgate magnetic field sensors (Stefan Mayer Instruments FL1-100) were mounted on the In-Ring and Reference positions. These sensors replaced the originally proposed AlphaLab Milligauss Magnetometer due to their higher resolution (20 $pT/Hz^{0.5}$ at 1 Hz) and stability.

All elements, including the magnetic field sensor, were fixed using the STYCAST 2850FT two component vacuum compatible epoxy glue. The cables were fixed using Teflon tape. The completely assembled sensor structure is shown in Figure 2.2-2 (left). Next, the Multi-Layer-Insulation (MLI) was carefully wrapped around the structure and again fixed with Teflon tape.

Then, LEMO connectors were mounted and sealed, the cables soldered to the connector, and all sensors were finally checked. Afterwards, the complete vacuum chamber was assembled and connected to a roughing pump-turbo pump system using the pump-out port (see Figure 2.2-3). The vacuum chamber was evacuated over night until a pressure of $3x10^{-6}$ mbar was reached. In addition, before the final pump down, no leaks were detected using a Helium leak detector.

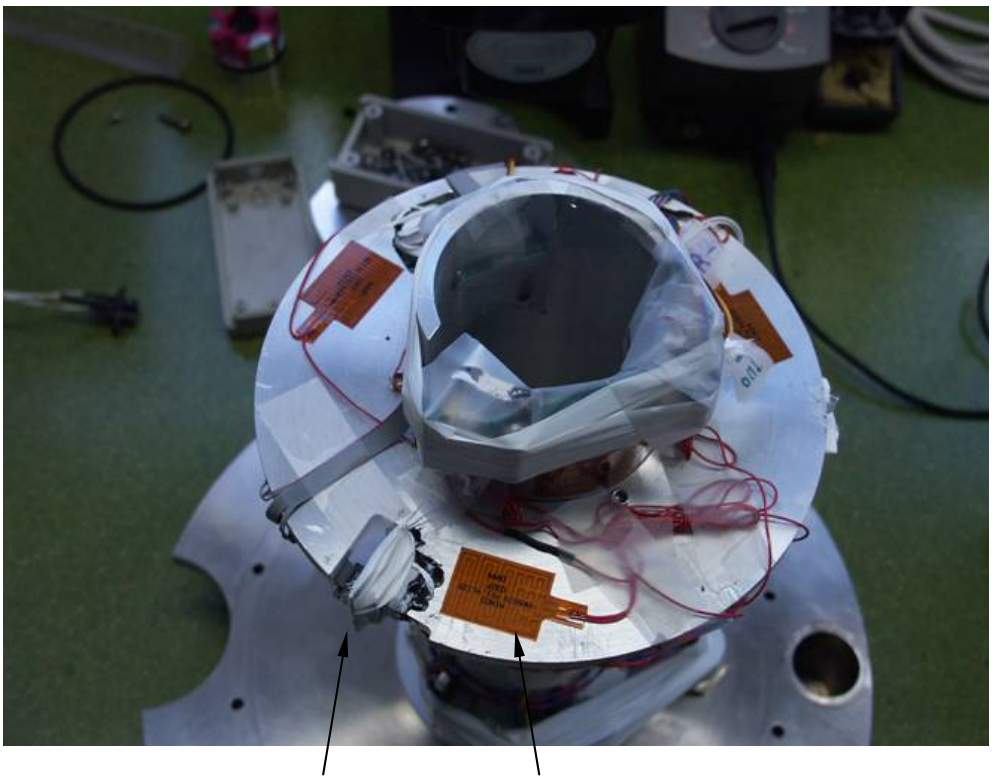

Figure 2.2-1 Accelerometers and Kapton Heater Foils Mounted on Structure

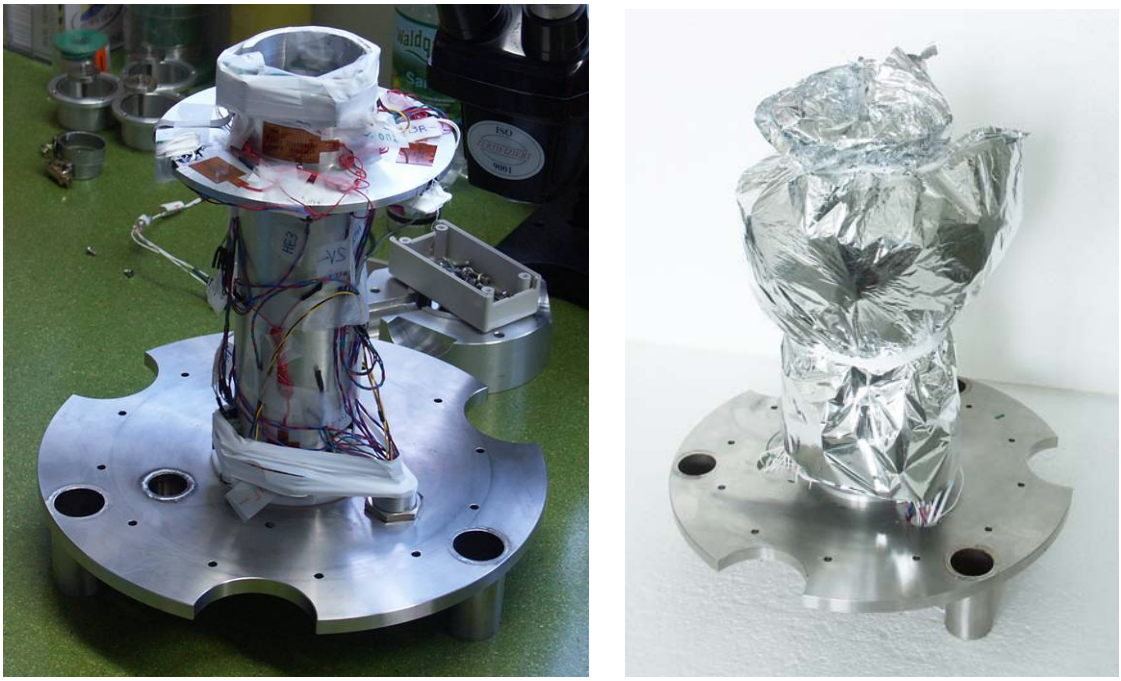

Figure 2.2-2 Complete Assembly of Accelerometers, Heaters, PT-100s and Magnetic Field Sensor on Structure (Left) and Wrapped in MLI Insulation (Right)

Figure 2.2-3 Completely Assembled Vacuum Chamber

2.3 Damping System

The following section explains the assembly of the original damping system – which was later replaced by the fixed structure.

First, the flange assembly with the radiation shields was assembled (see Figure 2.3-1). Then, the radial dampers that go to the copper ring were mounted (see Figure 2.3-2). A wire was used to pre-squeeze the spring and release it after the next sub-assembly.

Next, the copper ring with its radial dampers that go on the sensor vacuum-chamber was assembled (see Figure 2.3-3). Then, the copper ring was mounted on the flange, which is the first stage of the damping system (see Figure 2.3-4). Teflon hollow shafts were put inside the springs as a support to avoid jumps of the copper ring and to bring it to the center position. These Teflon shafts are believed to be most likely responsible for the large noise detected as they transmit part of the cryostat vibrations to the sensors.

Finally, the sensor-vacuum chamber was mounted as shown in Figure 2.3-5.

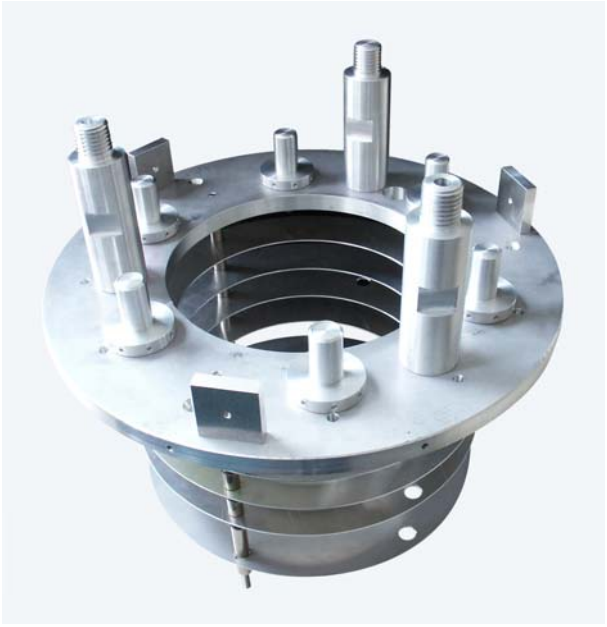

Figure 2.3-1 Flange Assembly

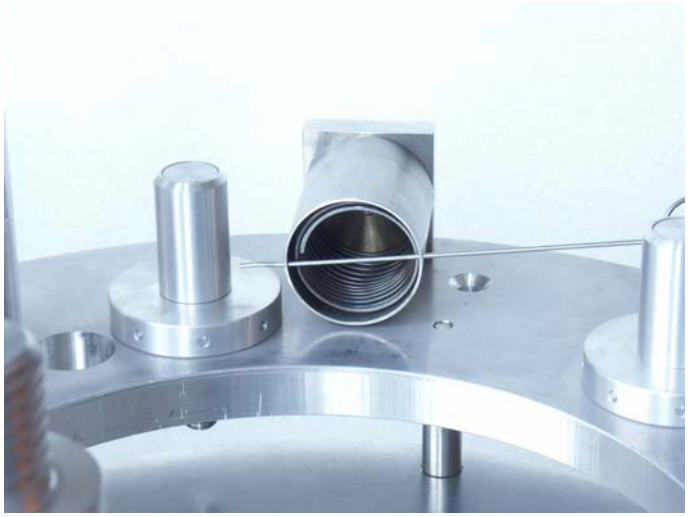

Figure 2.3-2 Flange Radial Damper

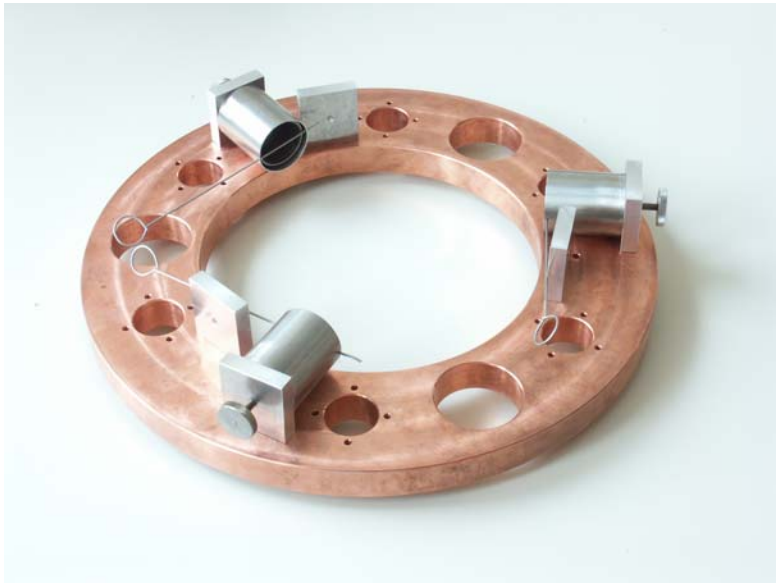

Figure 2.3-3 Copper Ring Assembly

Figure 2.3-4 Copper Ring-Flange Assembly (With Shaft and Superconductor Support Structure)

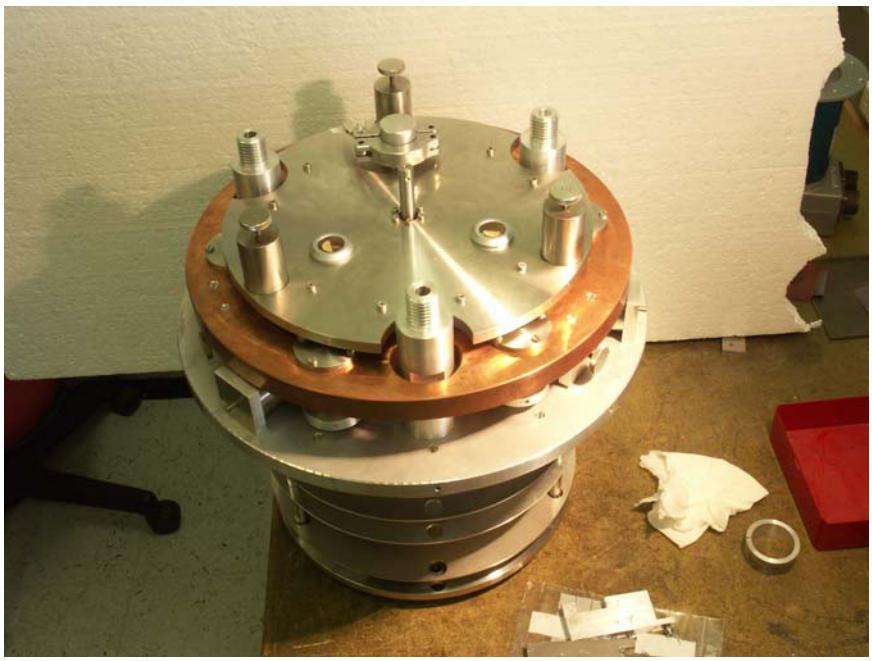

Figure 2.3-5 Complete Damping System Assembly

2.4 Motor and Coil Assembly

In order to test the assembly before mounting it on the cryostat (to avoid possible damage), the flange was mounted on a wood plate fixed to two tables. Figure 2.4-1 shows the assembly mounted on the plate with the motor axis, bearing and coupling. Figure 2.4-2 shows the coil mounted on the bottom. The superconductor supporting structure is inside the coil. Finally, Figure 2.4-3 shows the motor mounted on top of the assembly.

Figure 2.4-1 Motor Axis, Bearing and Coupling Assembly

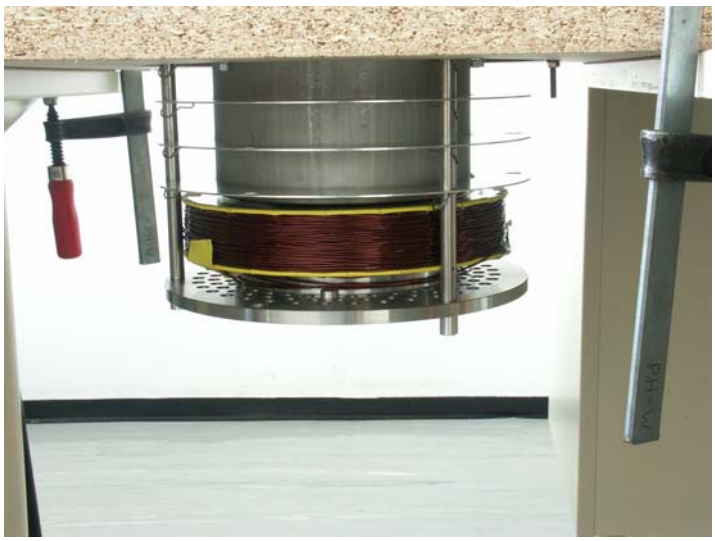

Figure 2.4-2 Coil Assembly

Figure 2.4-3 Motor Assembly

This assembly was tested with engine speeds up to 6500 rpm (minimum requirement 3000 rpm) and accelerations up to 1300 s^{-2} (minimum requirement 200 s^{-2}). No vibrations or abnormal facility behavior was notices although the apparatus worked at more than twice its minimum requirements. Therefore, it was concluded to mount the facility on the cryostat.

In addition to the electric motor, a compressed air motor was also purchased and tested with the facility in order to exclude any electromagnetic interference of the engine with the measurement. The engine chosen was a Düsterloh PMW 400 Z24 ML/MR. This engine can reach 4000 RPM with a pressure of 10 bar. It is manually controlled and the actual speed is measured using a custom-built optical encoder.

2.5 Superconductor Support and Axis

After the first tests with the BSCCO superconductor, the ceramic broke into pieces as it could not withstand the applied accelerations. Therefore, a new superconductor was purchased and glued into the support structure using STYCAST epoxy (see Figure 2.5-1). On the top of the axis, a standard bearing was mounted with a heater to maintain 25°C during operation. On the bottom of the axis, a low-temperature KOYO bearing was initially mounted according to the original design. During testing it was realized that the high speeds more or less immediately damaged the KOYO bearing. It turned out that the best solution was to use a standard bearing with the highest possible gap, remove any lubricant, and put carbon powder inside as a solid lubricant. This bearing survived all later tests.

Figure 2.5-1 Superconductor Support (Left) and Upper Bearing (Right)

In order to obtain a reliable temperature measurement, a silicon diode (DT-670B-SD) from Lakeshore was installed on the superconductor support structure. A miniature collector ring (MD6038 and MD6043 from LTN Precision Products) on top of the axis enabled the correct readout even during high speed rotation (see Figure 2.5-2). The temperature stayed within 0.1K at speeds up to 6500 RPM.

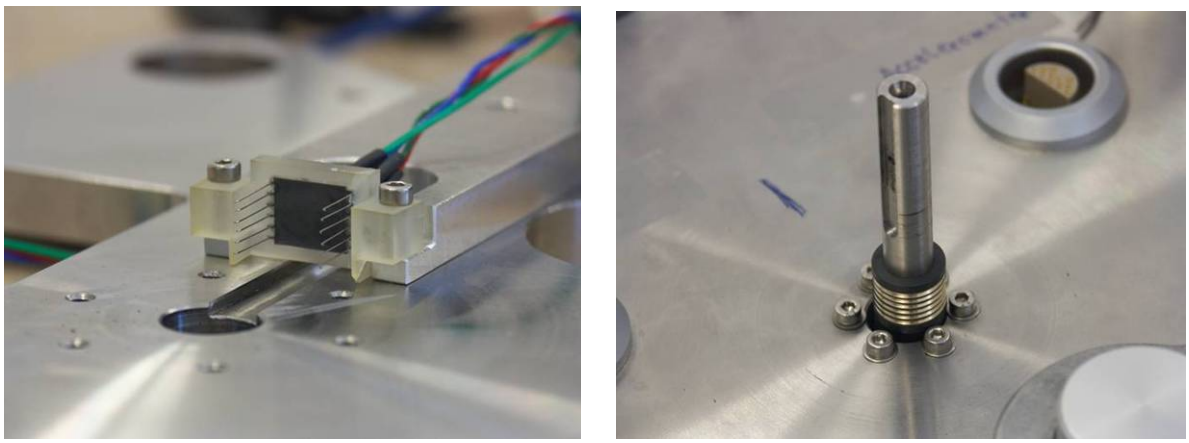

Figure 2.5-2 Miniature Collector Ring for Superconductor Temperature Read-Out

2.6 Cryostat Assembly

The experiment was then mounted on the cryostat (see Figure 2.6-1). In order to reduce possible vibrations from the motor, the cryostat was then put inside a box filled with sand. This increases the base weight by 1500 kg (see Figure 2.6-2).

Figure 2.6-1 Cryostat Assembly

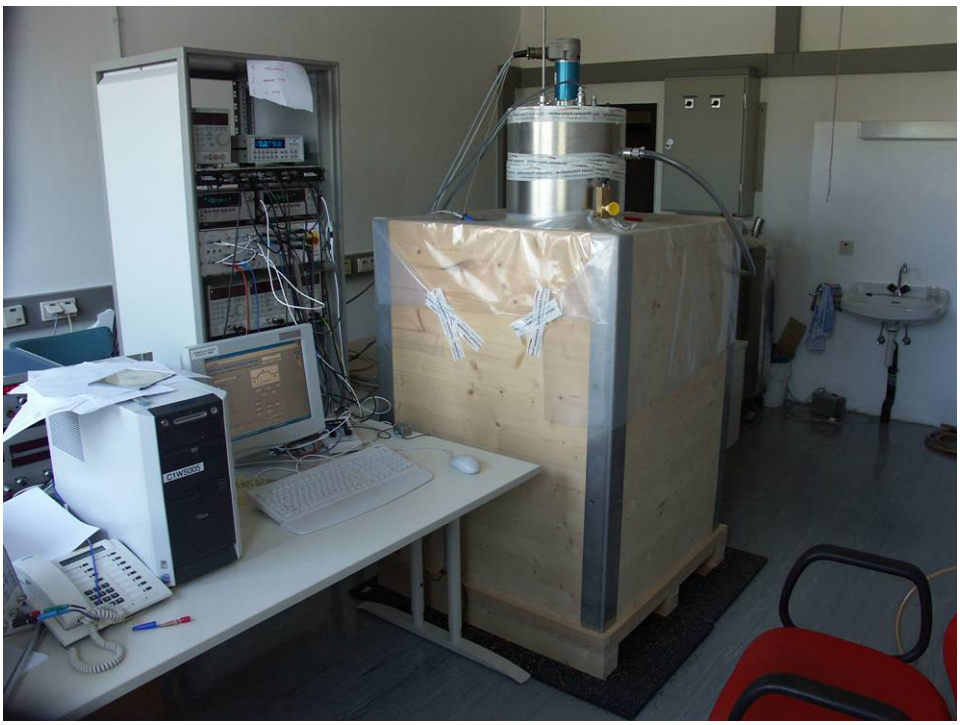

Figure 2.6-2 Cryostat Assembly in Sand Box

Because the noise level in this setup was too high (mN level), the original damping system had to be replaced. Tests with accelerometers on the floor during operation of the machine showed that the building very effectively damps the oscillations from the rotating superconducting ring. Therefore, a new design was made where the sensor chamber is directly mounted to a fixed structure made out of steel that is fixed to the floor and roof of the building (see Figure 2.6-3). Only flexible tubes along the three shafts (necessary to seal the cryostat) and electric wires from the sensor chamber to the flange have direct contact between the sensor chamber and the cryostat. This system proved to enable low noise operation during high rotation. The final configuration is shown with the air and electric motor in Figure 2.6-4.

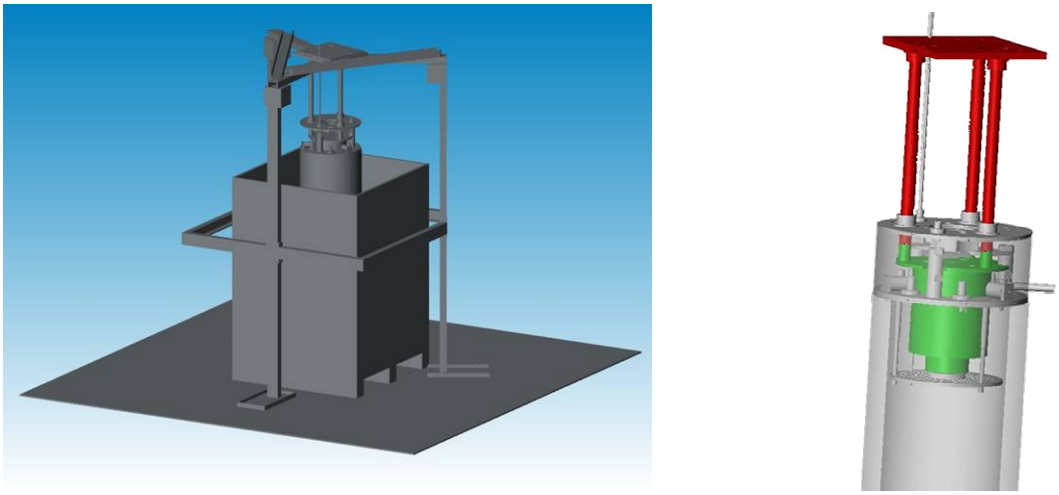

Figure 2.6-3 Fixed Structure around Cryostat holding the Sensor Chamber (Green) by three solid shafts (Red) - Shown in Detail on the Right

Figure 2.6-4 Final Configuration with Air Motor (Left) and Electric Motor (Right)

2.7 Electrical Setup

Figure 2.7-1 shows the setup of all sensors and electrical measurement devices. The accelerometers/magnetometers, the heaters as well as the low temperature monitor are controlled via the GPIB bus. The electric motor, the coil, the PT-100 temperature sensors and the optical encoder are controlled using a National Instruments DAQ board. The PC runs a LabView software to control and monitor all parameters.

Before the Keithley Nanovoltmeters, the sensors can be connected to an electronic box that subtracts two signal lines from each other (e.g. In-Ring Tangential – Reference Tangential Position). The differential signal can then be connected to the Keithley. Also a mixture of single and differential signals can be connected.

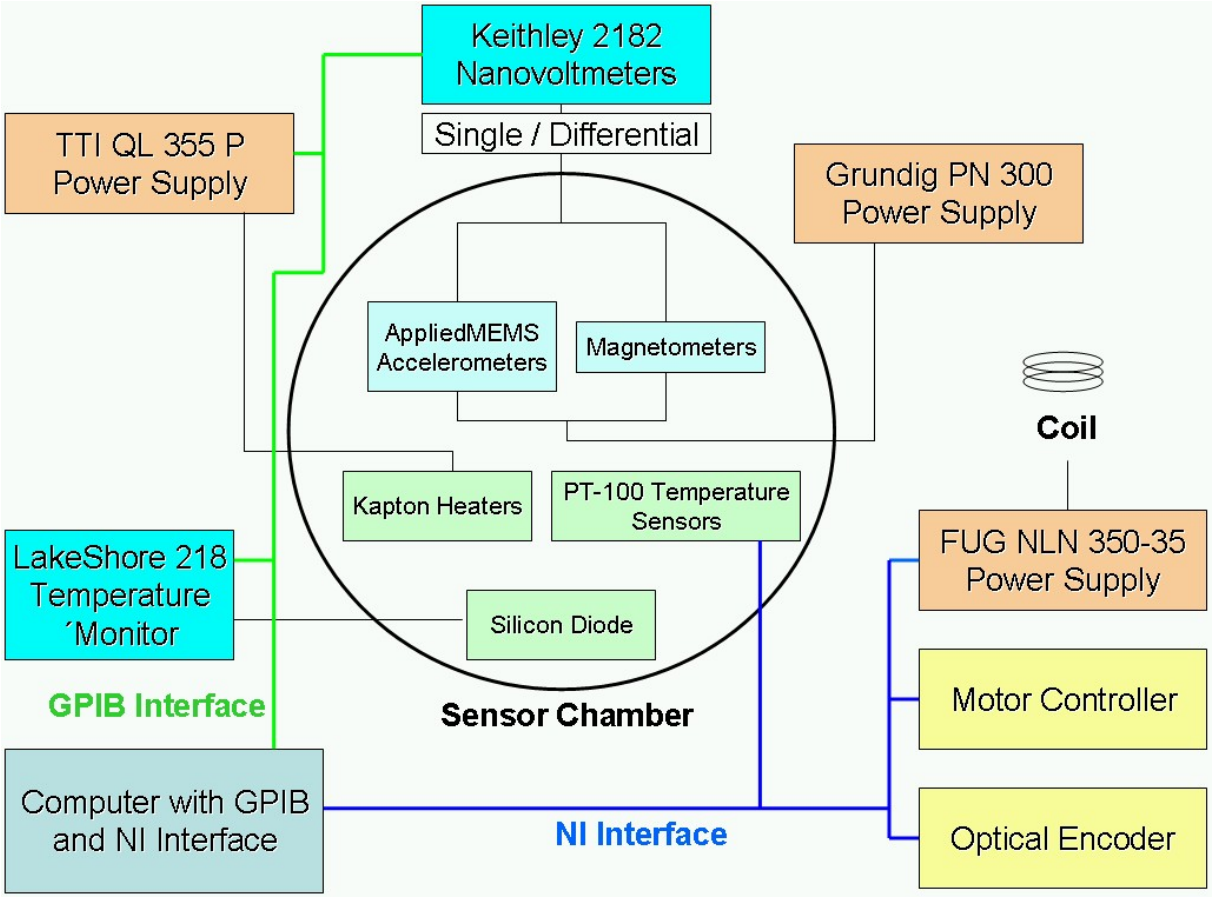

Figure 2.7-1 Electrical Setup

2.8 Data Acquisition and Control Program

In order to read out all sensors, command the motor and regulate the temperature at the bearing and accelerometers, a custom program was written in LabVIEW 7.1.

The following input parameters are processed by the program:

- 2x Keithley Nanovoltmeter, translated into gravitational acceleration (2V = 1 g) or magnetic field; digital integration and moving filter settings can be commanded via GPIB interface
- PT 100 thermocouple at all accelerometer positions (1x reference, 1x inner ring, 1x above ring); 2 wire method
- PT 100 thermocouple at upper bearing – 2 wire method
- Temperature superconductor (silicon diode connected via LakeShore 218 temperature monitor) [K]
- Field coil power supply
- Electric motor angular velocity and torque
- Optical encoder velocity

The following output parameters are processed by the program:

- Regulate heating power for each accelerometer and upper bearing position (according to temperature measured at each position)
- Drive field coil power supply
- Drive motor encoder

The program is subdivided into 6 main screens:

- Experiment: To set the profile shapes and speeds and to start the measurement (see Figure 2.8-1).
- Measurement: To define which accelerometer/magnetometer positions are connected to the Keithley Nanovoltmeters and which filter settings shall be used (see Figure 2.8-2 Left).
- Coil: To define the magnetic field (constant or profiles) that shall be produced from the coil.
- Environment: To set the temperature to which the accelerometers/upper bearing shall be controlled (see Figure 2.8-2 Right).
- Channels: Setup for GPIB and NI controller.
- Settings: Individual calibration constants for accelerometers and magnetometers.

Before each measurement, the Keithleys are calibrated and a 5 seconds test run is done to ensure that all data channels are synchronized. By using a frequency generator for one data channel it was verified that all channels are recorded with a maximum time shift of one timestep between them.

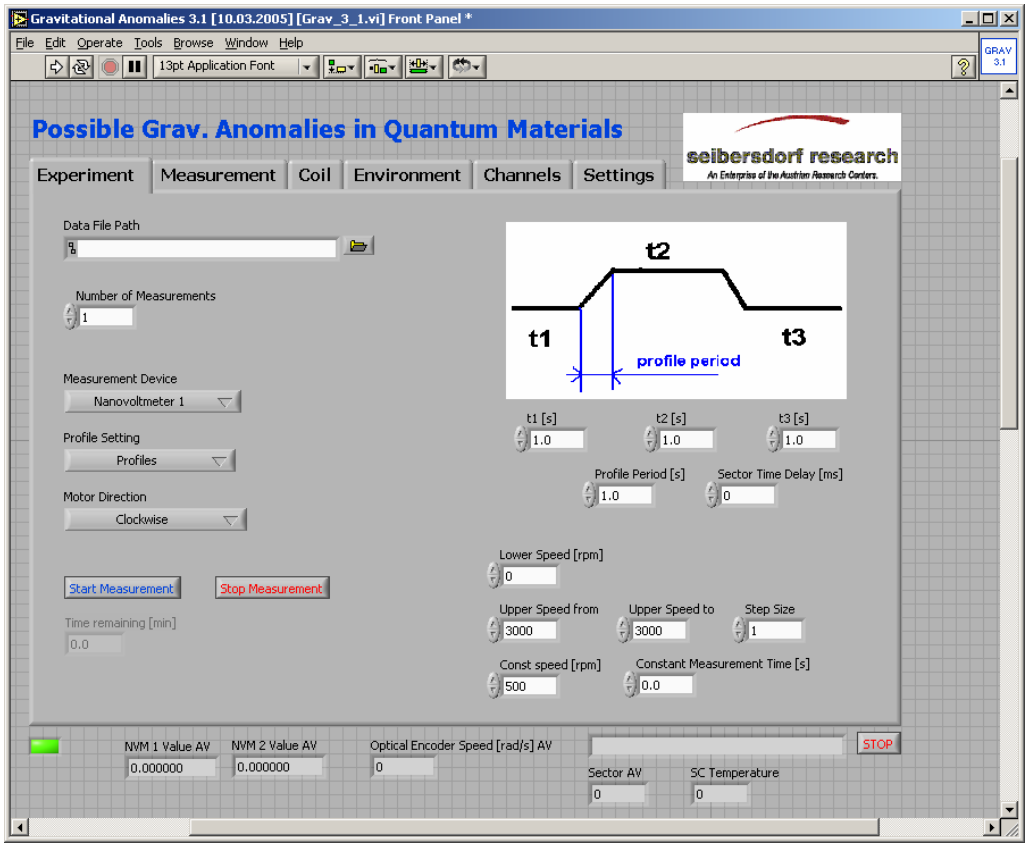

Figure 2.8-1 Experiment Screen

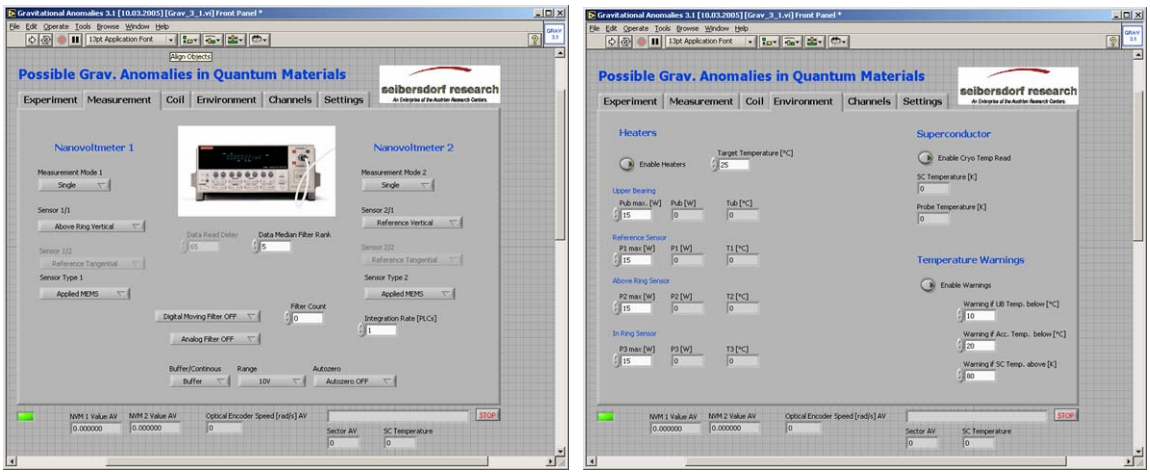

Figure 2.8-2 Measurement and Environment Screen

The speed and acceleration profile can be controlled as shown in Figure 2.8-3 by subdividing it into 5 sectors. Each sector speed and time interval can be set individually. For comparison, the raw data from the optical encoder is compared with the filtered (Digital Moving Filter over 5 data points) and commanded speed/acceleration. The noise of the raw data in the acceleration profile is due to the numerical differentiation. By comparison between commanded and measured speeds, the maximum deviation was < 5% at speeds up to 1000 RPM and < 1% at full speed.

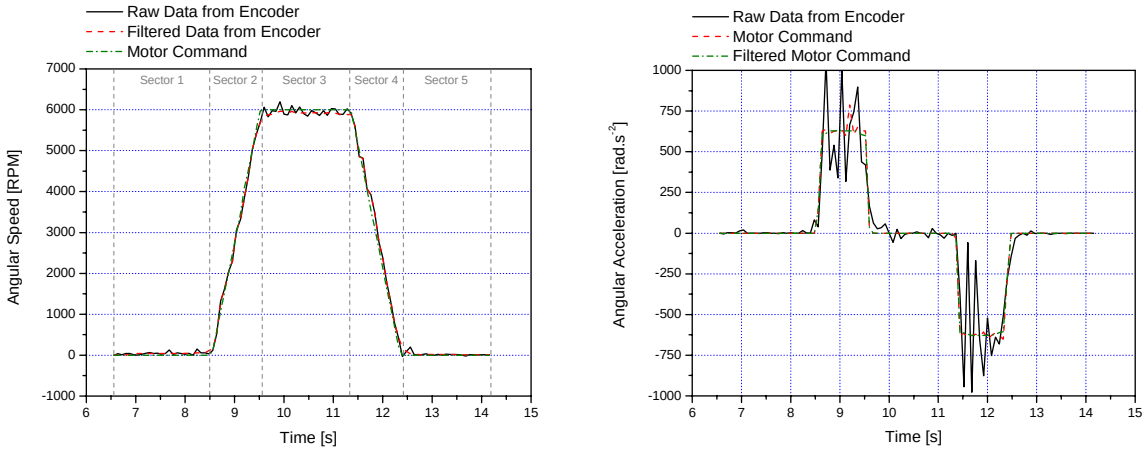

Figure 2.8-3 Speed and Acceleration Profile

2.9 Data Analysis Program

A second LabView program was also written (see Figure 2.9-1) in order to process the raw data and to do a statistical evaluation. The program can evaluate the coupling factors by performing a linear fit between the gravitational field measured and the applied speed, speed^2 and acceleration to the superconductor during each profile. As we always measure a number of profiles, the program can evaluate the coupling factors, the mean values and standard deviation, as well as the correlation factors. Other features include

- Selection of temperature, speed and acceleration range
- Selection of sectors (e.g. only sector 2 and 4)
- Subtraction of friction forces in the measurement (friction if proportional to the angular speed)
- Software subtraction of sensor positions

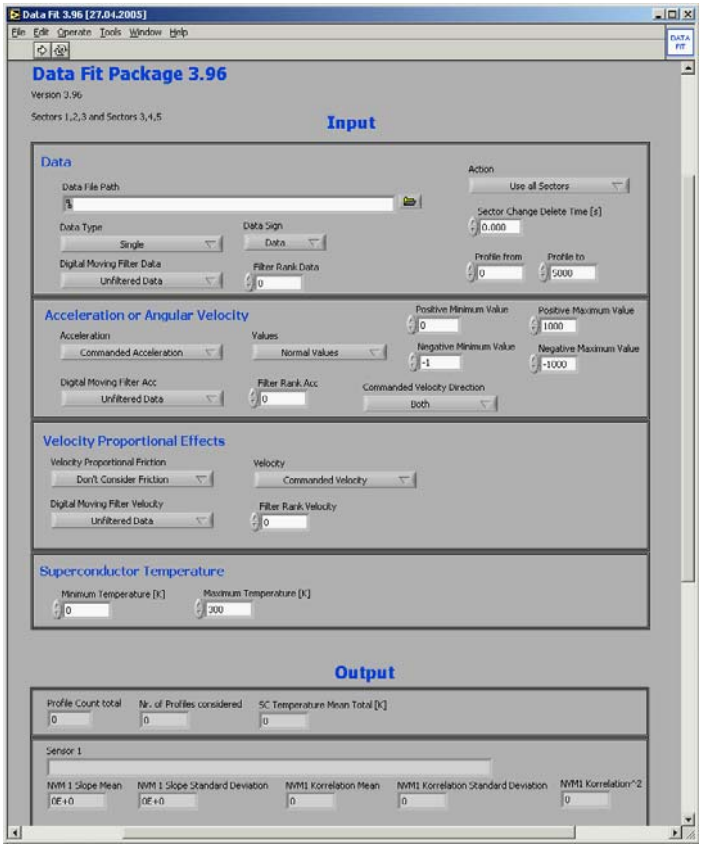

Figure 2.9-1 Data Analysis Program

3 EXPERIMENTAL RESULTS

3.1 Introduction

The following chapters summarize the experimental work carried out with the facility in its highest resolution configuration. In addition to a BSCCO superconductor, also experiments with YBCO were performed both a room temperature and at 77 K (using liquid nitrogen). For calibration purposes, also a Niobium ring was tested at 77 K (not superconductive at this temperature) in order to check for effects that could be caused by the liquid nitrogen itself.

In all tests, the following profile was commanded to the electric motor:

- 1 second at zero speed
- 1 second accelerating to 6500 RPM in clockwise direction
- 1 second remaining at full speed
- 1 second de-accelerating to zero speed
- Do the same profile but this time in counter-clockwise direction

This was repeated 5-10 times. Each profile was then processed using the DataFit Software and statistics were done to evaluate the coupling factors for all sensor positions inside and above the ring (using differential measurement technique). In addition to the angular acceleration coupling factor, also a possible coupling factor for the angular speed and angular speed^2 (centrifugal acceleration) was evaluated.

In order to perform the tests at 77 K, the cryostat was filled with liquid nitrogen to about 1 cm below the upper edge of the superconductor ring. After each profile, nitrogen evaporated and the liquid nitrogen level in the dewar was reduced. After about 70 profiles, the liquid was below the ring and the superconductor heated up.

3.2 Sensor External Influence

In order to reach the highest accuracy, the motor speed and acceleration was set to their limits. In all final runs, a top speed of 6500 RPM accelerated and de-accelerated in 1 s could be achieved. The first months of testing were devoted to run the machine with the BSCCO superconductor at 77K using liquid nitrogen and at near room temperature, analyze the signals, and to find if the motor or the setup are inducing false signals. The following three error sources were identified and consequently removed for the final runs:

1. The most severe problem was that after some time (ranging from minutes to hours, depending on the bearing) the bottom bearing started to get problems and created noise. This noise was proportional to ω^2 – the higher the force on the bearing, the higher the noise. This acoustic noise caused the cryostat and the fixed cage structure to vibrate. Due to the vertical mounting of the sensor chamber, the sensors could then also vibrate in the radial direction. This in turn was interpreted by the sensor electronics as a shift in the signal of the radial sensor (see Figure 3.2-1). This shift was several hundred µg (up to milli-g when the bearing was nearly dead), which then also transmitted to other sensor positions as they are not perfectly aligned to the central axis. The problem was circumvented by using a new bearing for every new test. As soon as the false signal appeared, the test had to be stopped and the bearing had to be exchanged. A similar problem occurred with the air motor as already the motor's noise was very large.

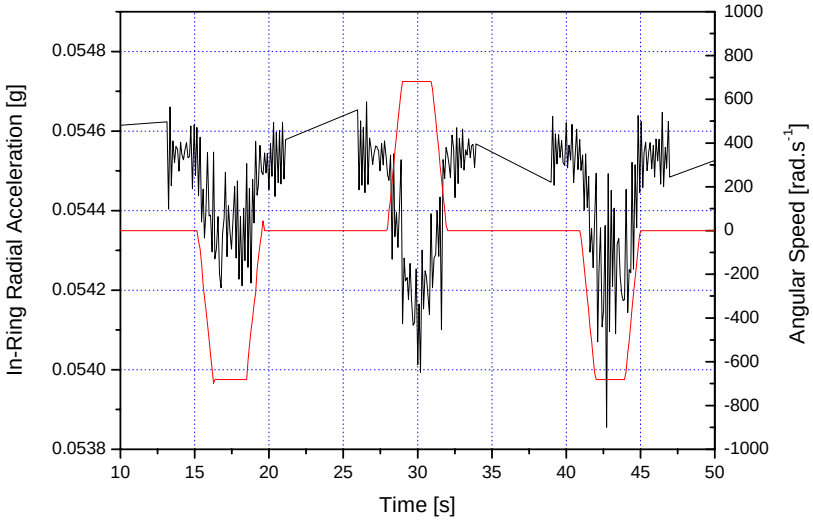

Figure 3.2-1 False Radial Measurement due to Bearing Noise

2. The second important point was that ice formation could occurred after some hours of liquid nitrogen cooling which then in turn could cause vibrations on the sensor chamber (the gap between axis and sensor chamber is only 1 mm!). This caused wrong signals in the radial direction because there was now a direct transfer of force from the rotation of the axis (a force again in the radial direction proportional to ω^2 appeared due to the centrifugal force on the axis, see Figure 3.2-2).

The best results were always obtained shortly after assembly and cooling down. It was found out that up to 5 hours after initial LN_2 filling, no false signals appeared.

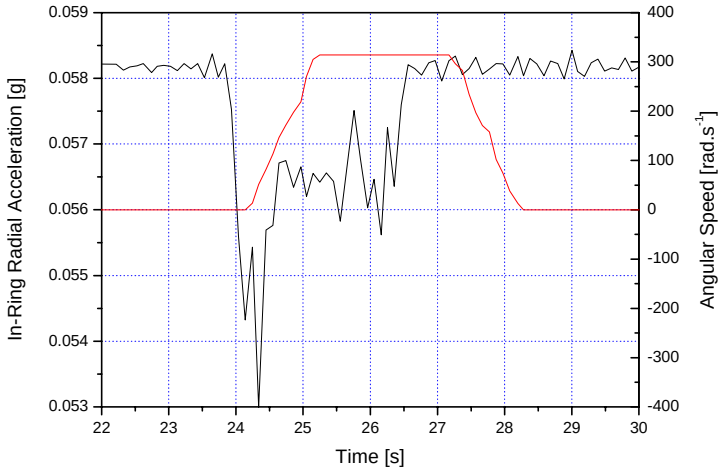

Figure 3.2-2 False Radial Measurement due to Ice Formation on Motor Axis

3. The third important point was to ground all cables that are not used and are coming from the sensor chamber. Because we had only two Keithley Nanovoltmeters, two sensors could be measured and the others signal outputs were initially floating. This caused a measurable influence of the motor magnetic field which was different if the BSCCO was superconductive or not (it acts like a magnetic mirror when it is superconductive). The motor on/off as well and the difference when the BSCCO was superconductive or not can be seen in Figure 3.2-3. After all cables were properly grounded, no influence could be seen any more.

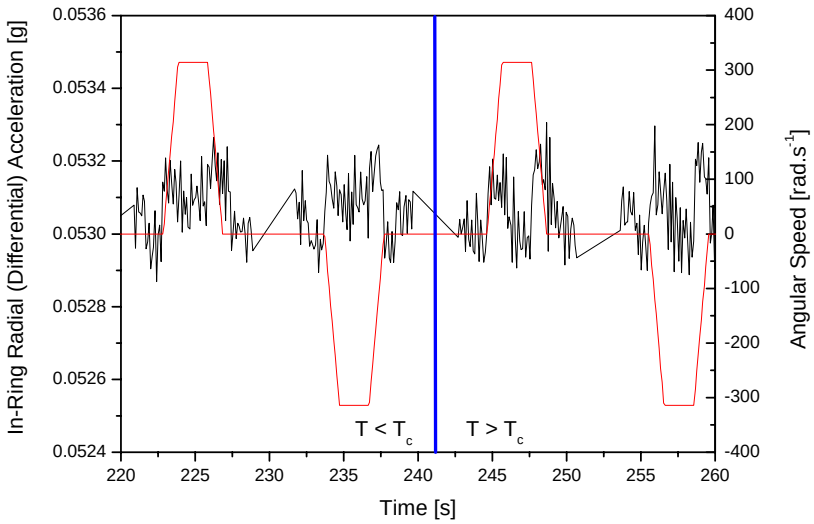

Figure 3.2-3 False Radial Measurement due to Cable Induction

Using the coil, the influence of a strong magnetic field on the accelerometers was evaluated. The test was done with the BSCCO ring at 117 K (normal conductive) and 77 K (superconductive). An oscillating magnetic field with an amplitude of 20 mT was applied and the sensor responses were evaluated (see Figure 3.2-4 to Figure 3.2-9). Table 3 summarizes the measured offsets, which were linear with the applied magnetic field, when the BSCCO is superconductive, it acts as a magnetic shield and reduces the influence on the sensors.

As the maximum magnetic field from the electric motor was measured to be about 50 µT, the maximum offset for the real runs should be therefore less than 0.025 µg, which is far below the measurement threshold of the sensors (about 1 µg). Therefore, influence of magnetic fields on the results can be neglected.

	Offset [µg]	
Sensor Position	Normal Conductive	Superconductive
In-Ring Radial	5	< 1
In-Ring Tangential	10	5
In-Ring Vertical	10	2.5
Above-Ring Radial	<1	< 1
Above-Ring Tangential	5	5
Above-Ring Vertical	5	10

Table 3 Magnetic Field Influence (20 mT) on Sensors

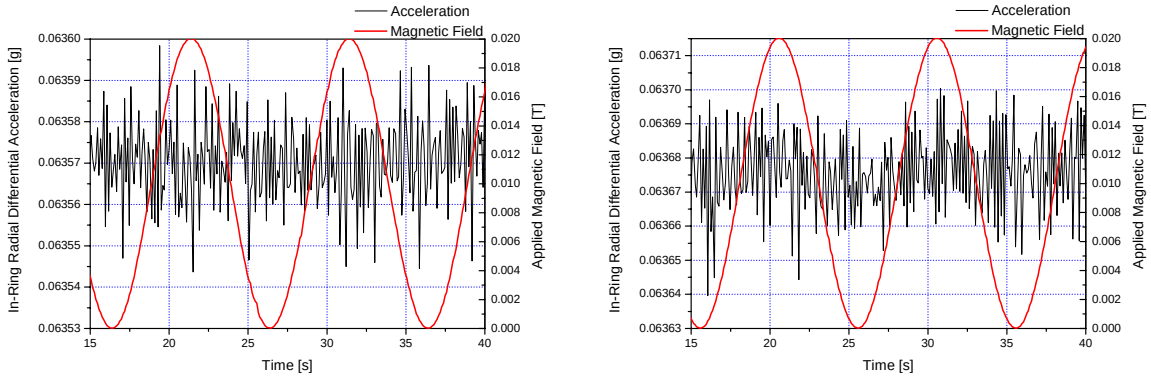

Figure 3.2-4 Influence of Magnetic Field on In-Ring Radial Sensor with BSCCO at 77K and 270K

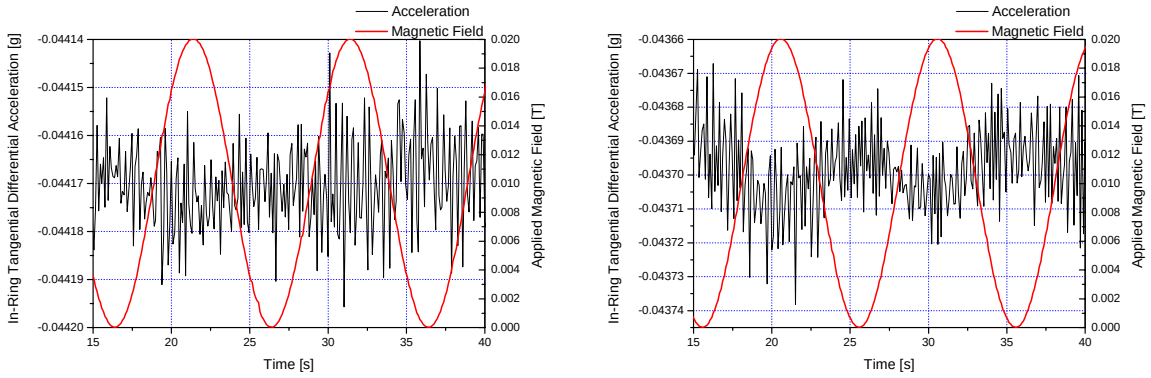

Figure 3.2-5 Influence of Magnetic Field on In-Ring Tangential Sensor with BSCCO at 77K and 270K

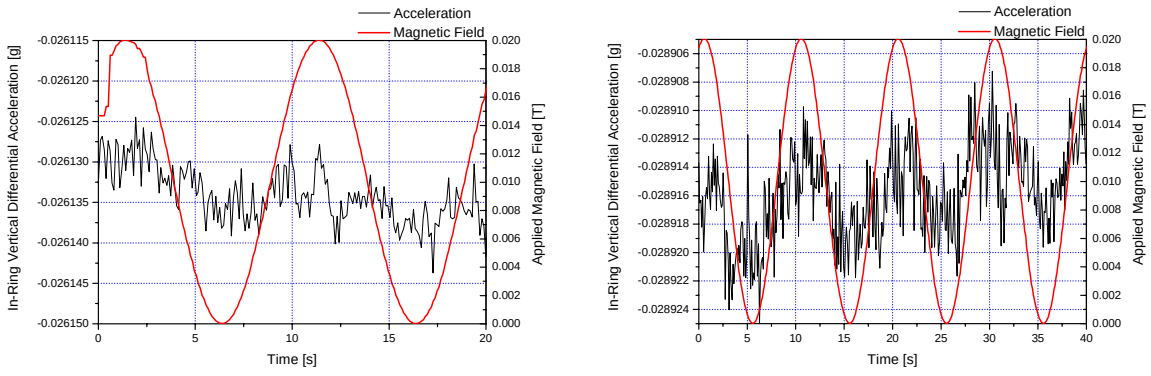

Figure 3.2-6 Influence of Magnetic Field on In-Ring Vertical Sensor with BSCCO at 77K and 270K

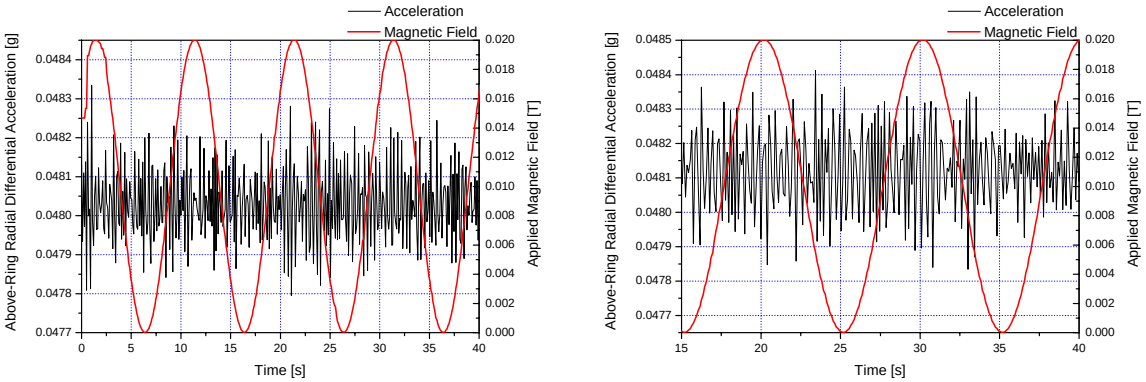

Figure 3.2-7 Influence of Magnetic Field on Above-Ring Radial Sensor with BSCCO at 77K and 270K

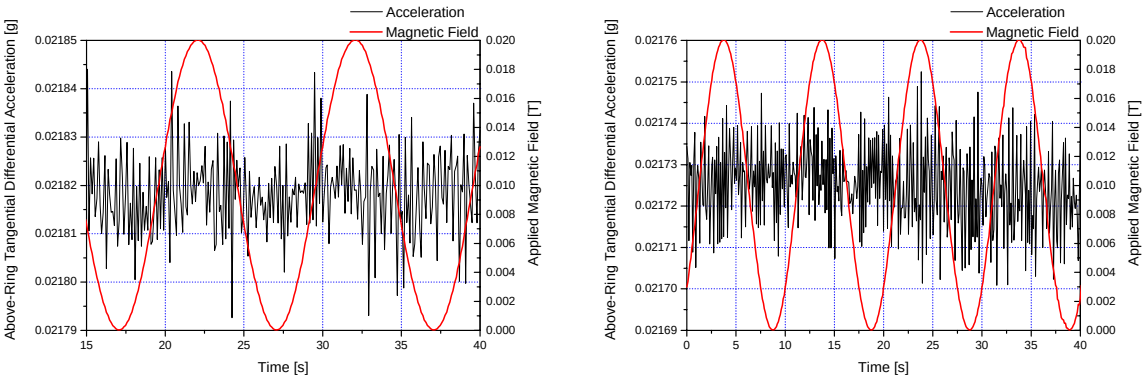

Figure 3.2-8 Influence of Magnetic Field on Above-Ring Tangential Sensor with BSCCO at 77K and 270K

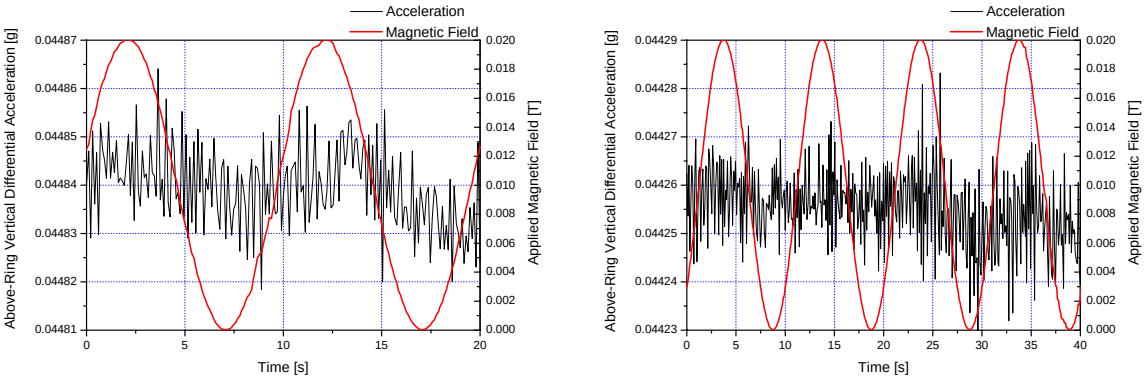

Figure 3.2-9 Influence of Magnetic Field on Above-Ring Vertical Sensor with BSCCO at 77K and 270K

3.3 Facility Calibration with Niobium Dummy

Figure 3.4-2 to Figure 3.4-7 show a comparison between all sensor positions at 77K and 270K during acceleration to maximum speed in both directions. The sensor sigma at our measurement rate of 10 Hz was about 15 µg as it can be seen in the raw data plots.

The coupling factors (linear fit of raw data per profile) between gravitational field and applied acceleration, velocity and velocity^2 for Niobium at 77K and 270K is shown in Tables 4-6.

No significant difference between 77K and 270K can be seen, therefore, the results of the facility are not influenced by the liquid nitrogen (evaporation during rotating, different acoustic noise of bearing when in or out of liquid nitrogen, etc.).

The angular acceleration coupling factor sigmas for all sensors are in the low 10^{-8} range, except for the vertical direction, which is in the low 10^{-9} range (due to the construction of the fixed cage, the vertical direction has the highest damping factor).

Comparing with the predicted coupling factors in Table 2, that is the right range to detect the anomaly based on Tate's measurement (for which the facility was designed in Phase I), but the sigmas are too high by at least 1-2 orders of magnitude to detect induced gravitational fields for high-temperature superconductors (due to the much lower Cooper-pair density).

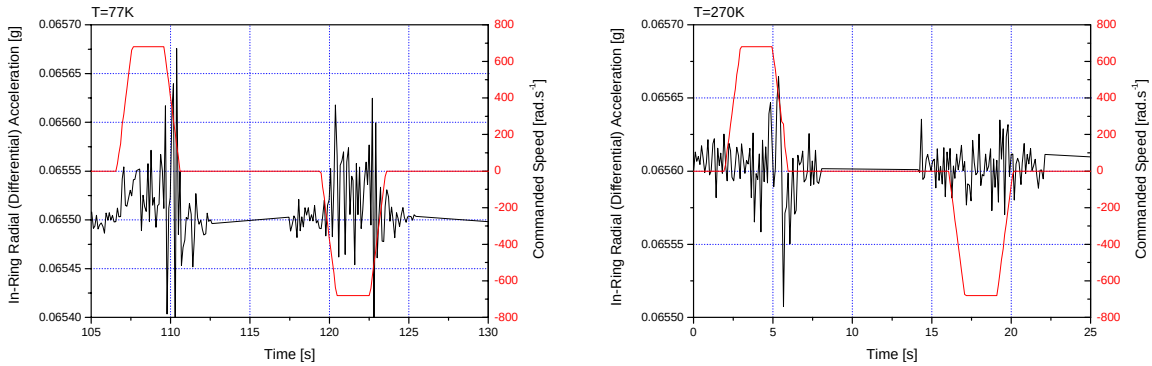

Figure 3.3-1 Niobium In-Ring Radial Differential Sensor Comparison at 77K and 270K

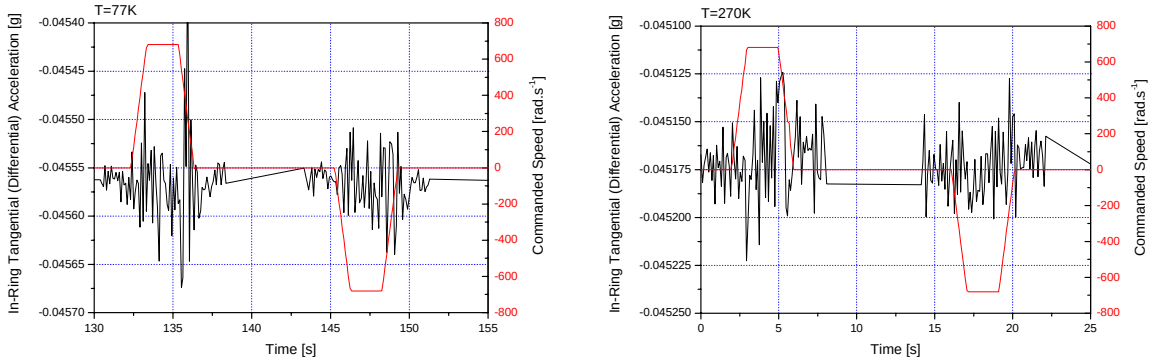

Figure 3.3-2 Niobium In-Ring Tangential Differential Sensor Comparison at 77K and 270K

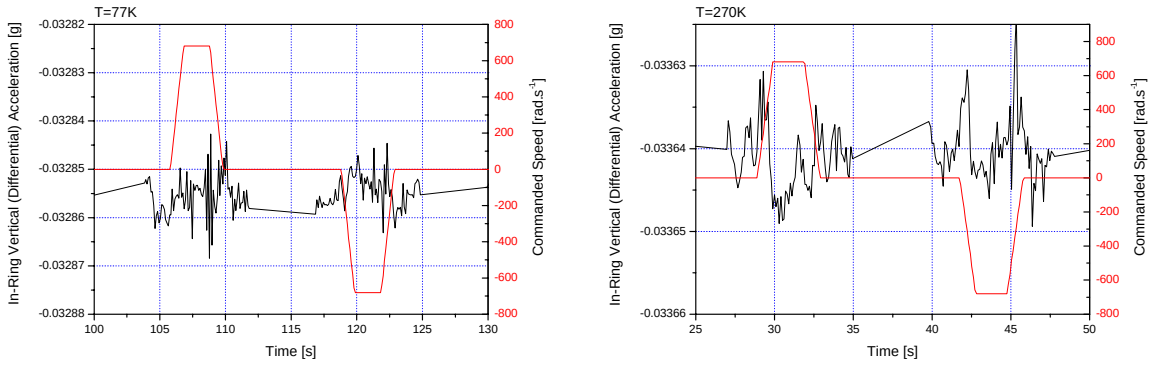

Figure 3.3-3 Niobium In-Ring Vertical Differential Sensor Comparison at 77K and 270K

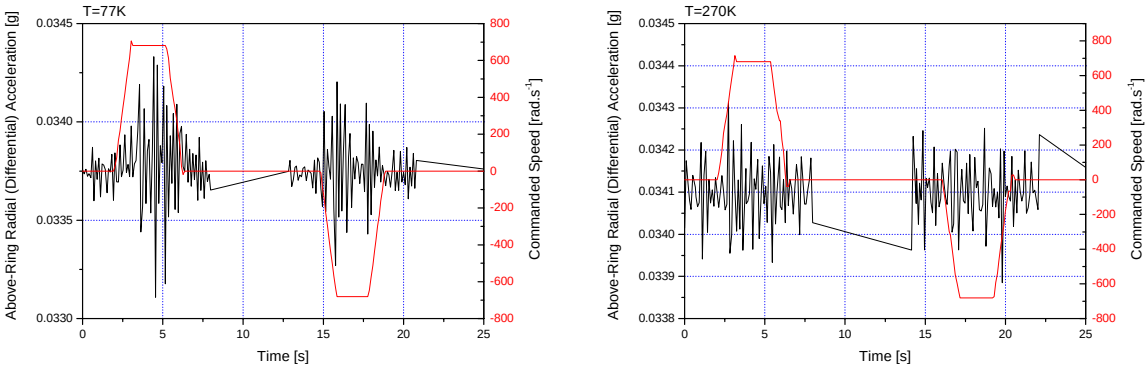

Figure 3.3-4 Niobium Above-Ring Radial Differential Sensor Comparison at 77K and 270K

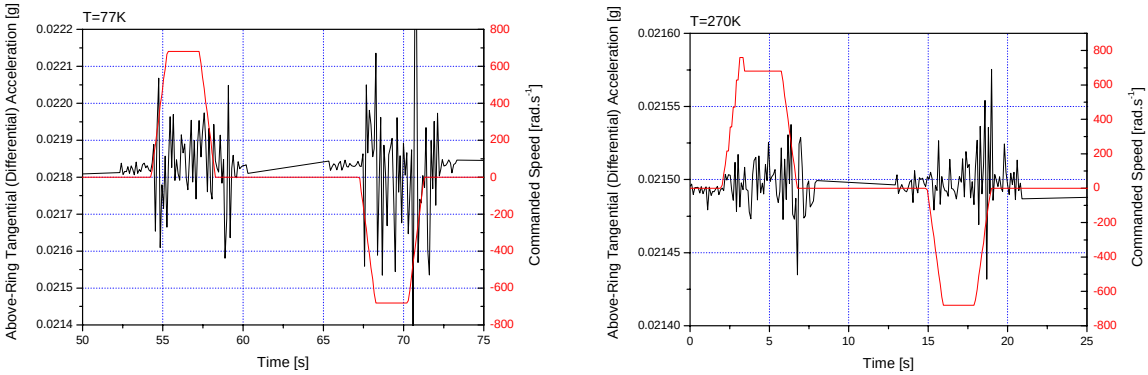

Figure 3.3-5 Niobium Above-Ring Tangential Differential Sensor Comparison at 77K and 270K

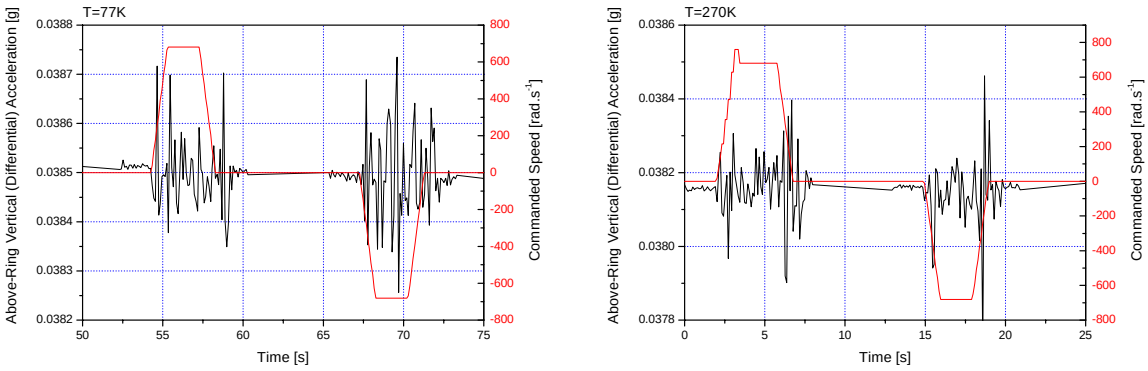

Figure 3.3-6 Niobium Above-Ring Vertical Differential Sensor Comparison at 77K and 270K

	77K				270K			
	Acceleration Coupling Factor		Correlation Factor		Acceleration Coupling Factor		Correlation Factor	
Position	**Mean**	**Sigma**	**Mean**	**Sigma**	**Mean**	**Sigma**	**Mean**	**Sigma**
In-Ring Radial	-6.21E-09	1.76E-08	-0.04	0.13	-1.80E-09	1.18E-08	-0.02	0.15
In-Ring Tangential	-1.29E-09	2.05E-08	-0.01	0.17	-2.53E-10	1.11E-08	0.00	0.15
In-Ring Vertical	-2.48E-10	1.42E-09	-0.02	0.13	9.85E-10	1.62E-09	0.08	0.14
Above-Ring Radial	-2.87E-08	3.36E-08	-0.04	0.05	1.15E-09	1.30E-08	0.00	0.04
Above-Ring Tangential	-1.01E-08	4.97E-08	0.00	0.10	-3.06E-10	8.88E-09	0.00	0.14
Above-Ring Vertical	5.42E-09	1.80E-08	0.03	0.08	-3.37E-09	4.62E-08	0.00	0.16

Table 4 Niobium Acceleration Coupling at 77K and 270K (Over 20 Profiles)

	77K				270K			
	Velocity Coupling Factor		Correlation Factor		Velocity Coupling Factor		Correlation Factor	
Position	**Mean**	**Sigma**	**Mean**	**Sigma**	**Mean**	**Sigma**	**Mean**	**Sigma**
In-Ring Radial	-9.55E-10	4.30E-09	-0.09	0.27	-1.65E-11	6.67E-09	0.00	0.07
In-Ring Tangential	-1.66E-08	7.02E-08	0.00	0.08	-9.85E-10	7.87E-09	0.00	0.11
In-Ring Vertical	-1.72E-09	3.13E-09	-0.15	0.26	-1.13E-09	5.44E-09	-0.05	0.42
Above-Ring Radial	-1.41E-08	6.61E-08	0.00	0.095	4.79E-11	7.58E-09	0.00	0.02
Above-Ring Tangential	8.96E-09	4.13E-08	0.02	0.11	-2.02E-09	7.69E-09	-0.04	0.11
Above-Ring Vertical	-4.92E-09	2.37E-08	0.00	0.07	-2.59E-09	1.84E-08	-0.01	0.08

Table 5 Niobium Velocity Coupling at 77K and 270K (Over 20 Profiles)

	77K				270K			
	Velocity^2 Coupling Factor		Correlation Factor		Velocity^2 Coupling Factor		Correlation Factor	
Position	**Mean**	**Sigma**	**Mean**	**Sigma**	**Mean**	**Sigma**	**Mean**	**Sigma**
In-Ring Radial	3.79E-12	4.93E-12	0.18	0.20	-2.73E-12	8.83E-12	-0.02	0.06
In-Ring Tangential	8.39E-11	4.00E-11	0.06	0.03	-8.63E-12	8.12E-12	-0.08	0.07
In-Ring Vertical	2.65E-12	4.09E-12	0.15	0.23	-8.55E-12	2.85E-12	-0.44	0.15
Above-Ring Radial	7.30E-11	4.70E-11	0.06	0.03	-3.37E-12	1.05E-11	0.00	0.01
Above-Ring Tangential	2.82E-11	5.22E-11	0.06	0.09	4.18E-12	9.11E-12	0.05	0.08
Above-Ring Vertical	1.16E-11	3.37E-11	0.02	0.07	-7.40E-12	2.70E-11	-0.01	0.08

Table 6 Niobium Velocity^2 Coupling at 77K and 270K (Over 20 Profiles)

3.4 BSCCO Coupling Factor Evaluation

In order to evaluate the critical temperature of our BSCCO ring (manufactured by NEXANS Superconductors, dimension 150x138x15 mm), a magnetic field was trapped during cooling down using the coil. Then the coil was switched off – and the magnetic field remained because BSCCO is a Type-II superconductor. During warming up, the magnetic field suddenly dropped to zero – exactly when the superconductor turned normal conductive. During several tests the critical temperature in our setup was therefore evaluated to be around 88.3 K (see Figure 3.4-1). This value is about 2 K higher than BSCCO critical temperatures in the literature (for phase 2122) which is probably due to our temperature measurement location of the silicon diode and the collector ring setup as well as the STYCAST fixing of the ring into the superconductor holder.

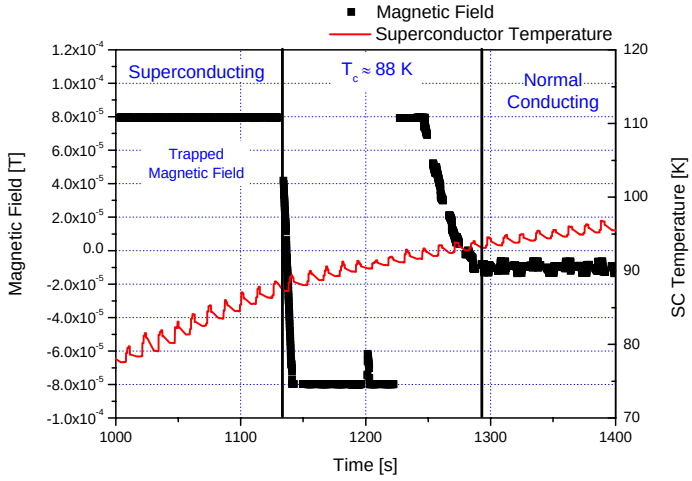

Figure 3.4-1 BSCCO Critical Temperature Measurement with Trapped Magnetic Field

Figure 3.4-2 to Figure 3.4-7 show a comparison between all sensor positions at 77K and 270K during acceleration to maximum speed in both directions. The sensor sigma at our measurement rate of 10 Hz was about 15 µg as it can be seen in the raw data plots.

The coupling factors (linear fit of raw data per profile) between gravitational field and applied acceleration, velocity and velocity² for BSCCO at 77K and 270K are shown in Tables 7-9. The sigmas are a little bit smaller compared to the Niobium dummy tests, probably due to the smaller weight of the ring and therefore reduced forces on the bearing.

For the acceleration coupling factors, all mean values are below its sigma. Also, no significant difference can be seen between the superconductive and normal conductive case – within the resolution threshold. The sigmas must be interpreted as upper boundaries for possible gravitational interactions for BSCCO.

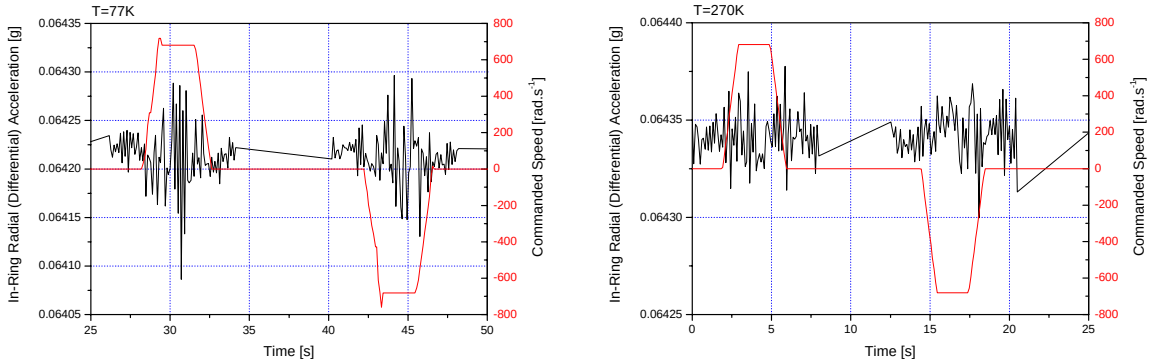

Figure 3.4-2 BSCCO In-Ring Radial Differential Sensor Comparison at 77K and 270K

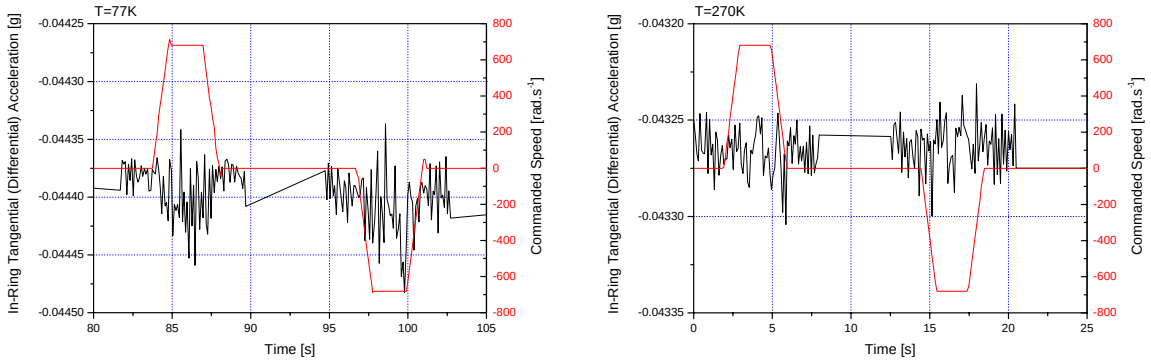

Figure 3.4-3 BSCCO In-Ring Tangential Differential Sensor Comparison at 77K and 270K

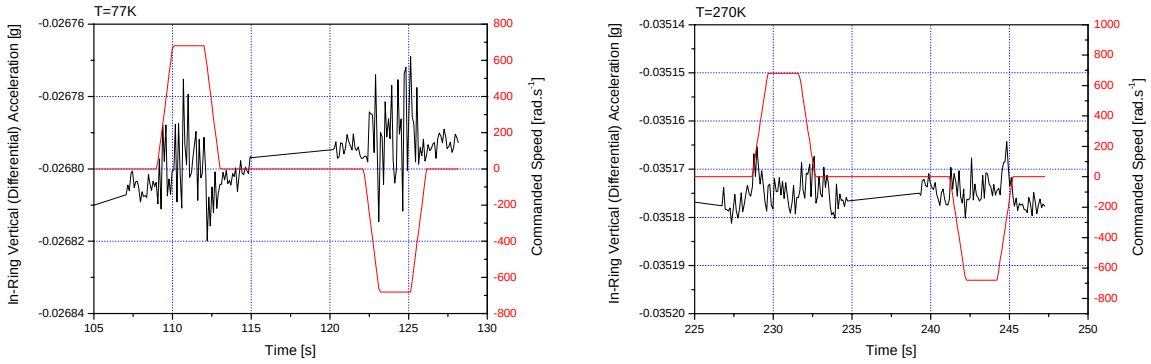

Figure 3.4-4 BSCCO In-Ring Vertical Differential Sensor Comparison at 77K and 270K

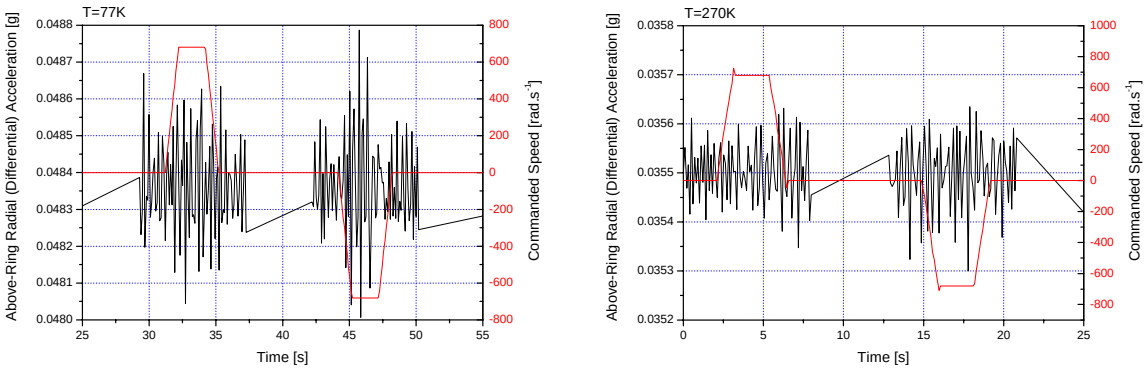

Figure 3.4-5 BSCCO Above-Ring Radial Differential Sensor Comparison at 77K and 270K

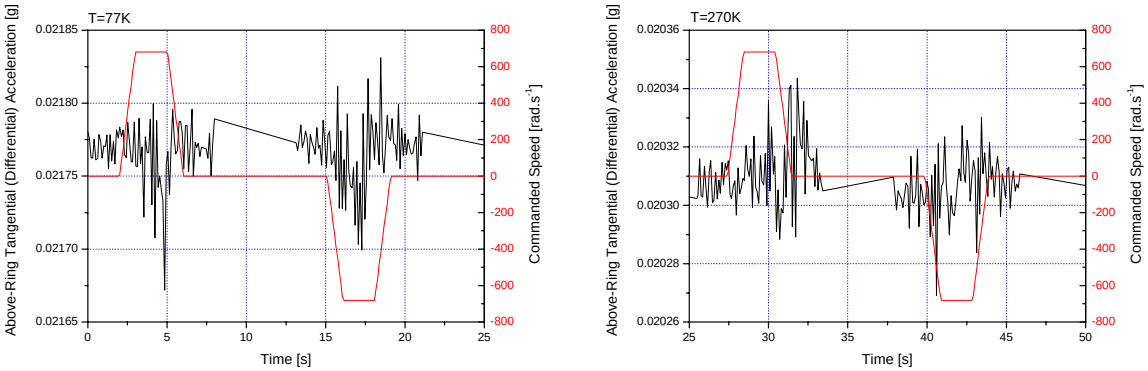

Figure 3.4-6 BSCCO Above-Ring Tangential Differential Sensor Comparison at 77K and 270K

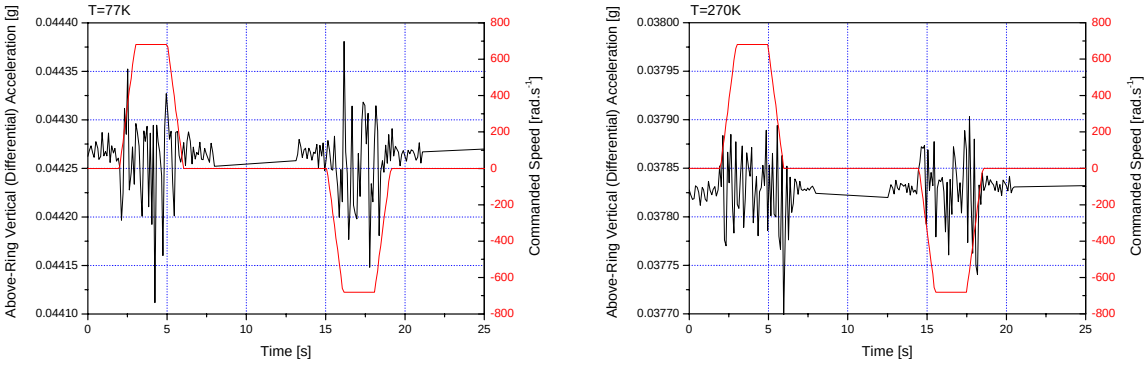

Figure 3.4-7 BSCCO Above-Ring Vertical Differential Sensor Comparison at 77K and 270K

	77K				270K			
	Acceleration Coupling Factor		Correlation Factor		Acceleration Coupling Factor		Correlation Factor	
Position	**Mean**	**Sigma**	**Mean**	**Sigma**	**Mean**	**Sigma**	**Mean**	**Sigma**
In-Ring Radial	-9.73E-10	8.45E-09	-0.01	0.11	-4.00E-09	5.34E-09	-0.09	0.12
In-Ring Tangential	-2.96E-09	4.84E-09	-0.04	0.06	-8.61E-10	5.51E-09	-0.02	0.14
In-Ring Vertical	4.52E-10	2.90E-09	0.02	0.13	7.59E-10	1.43E-09	0.07	0.14
Above-Ring Radial	2.06E-09	1.80E-08	0.00	0.04	1.14E-10	1.23E-08	0.01	0.04
Above-Ring Tangential	8.13E-10	7.01E-09	0.02	0.10	9.12E-09	8.09E-09	0.20	0.18
Above-Ring Vertical	9.23E-10	1.07E-08	0.00	0.12	2.87E-09	2.81E-08	0.02	0.24

Table 7 BSCCO Acceleration Coupling at 77K and 270K (Over 20 Profiles)

	77K				270K			
	Velocity Coupling Factor		Correlation Factor		Velocity Coupling Factor		Correlation Factor	
Position	**Mean**	**Sigma**	**Mean**	**Sigma**	**Mean**	**Sigma**	**Mean**	**Sigma**
In-Ring Radial	1.75E-09	1.20E-08	0.01	0.13	-3.27E-10	4.93E-09	-0.01	0.11
In-Ring Tangential	-7.07E-09	3.60E-08	-0.03	0.39	2.07E-09	4.88E-09	0.04	0.11
In-Ring Vertical	-3.40E-09	1.12E-08	-0.10	0.43	1.30E-10	2.49E-09	0.01	0.21
Above-Ring Radial	-2.13E-09	1.14E-08	-0.01	0.03	-1.28E-09	6.99E-09	0.00	0.03
Above-Ring Tangential	7.23E-10	3.55E-08	-0.03	0.44	1.56E-11	1.09E-08	-0.02	0.20
Above-Ring Vertical	-6.90E-09	2.08E-08	-0.07	0.19	-8.39E-10	1.31E-08	-0.01	0.11

Table 8 BSCCO Velocity Coupling at 77K and 270K (Over 20 Profiles)

	77K				270K			
	Velocity^2 Coupling Factor		Correlation Factor		Velocity^2 Coupling Factor		Correlation Factor	
Position	**Mean**	**Sigma**	**Mean**	**Sigma**	**Mean**	**Sigma**	**Mean**	**Sigma**
In-Ring Radial	-1.04E-11	1.22E-11	-0.08	0.08	4.98E-12	5.98E-12	0.07	0.09
In-Ring Tangential	-5.00E-11	1.35E-11	-0.37	0.10	2.06E-12	7.29E-12	0.03	0.11
In-Ring Vertical	1.34E-11	1.04E-11	0.35	0.25	6.47E-13	3.11E-12	0.04	0.18
Above-Ring Radial	3.62E-12	1.68E-11	0.01	0.03	5.69E-12	8.45E-12	0.02	0.02
Above-Ring Tangential	-5.00E-11	1.15E-11	-0.42	0.12	1.53E-12	1.55E-11	0.02	0.19
Above-Ring Vertical	-2.03E-11	2.54E-11	-0.12	0.17	6.46E-12	1.25E-11	0.04	0.07

Table 9 BSCCO Velocity^2 Coupling at 77K and 270K (Over 20 Profiles)

3.5 YBCO Coupling Factor Evaluation

The YBCO ring was purchased from ATZ and has a thicker wall thickness in order to properly seed and grow the crystals. The final size measured was 160x130x15 mm and the superconductor holder was adapted accordingly. Also in this case, trapped fields were used to evaluate the critical temperature of the YBCO ring. The tests showed that the critical temperature was about 92 K, consistent with results in the literature (see Figure 3.5-1).

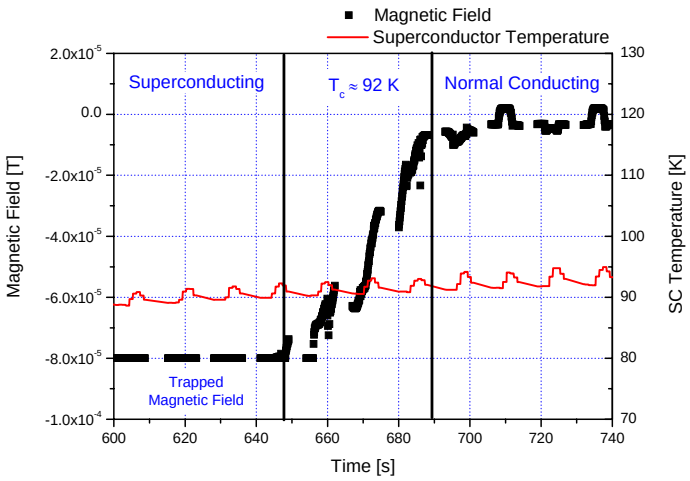

Figure 3.5-1 YBCO Critical Temperature Measurement with Trapped Magnetic Field

Figure 3.5-2 to Figure 3.5-7 show a comparison between all sensor positions at 77K and 200K during acceleration to maximum speed in both directions. The sensor sigma at our measurement rate of 10 Hz was about 15 µg as it can be seen in the raw data plots.

The coupling factors (linear fit of raw data per profile) between gravitational field and applied acceleration, velocity and velocity² for YBCO at 77K and 200K are shown in Tables 10-12. The sigmas are a little bit smaller compared to the Niobium dummy tests, probably due to the smaller weight of the ring and therefore reduced forces on the bearing.

The data is very similar to the BSCCO results. For the acceleration coupling factors, again all mean values are below its sigma. Also, no significant difference can be seen between the superconductive and normal conductive case – within the resolution threshold. The sigmas must be interpreted as upper boundaries for possible gravitational interactions for YBCO.

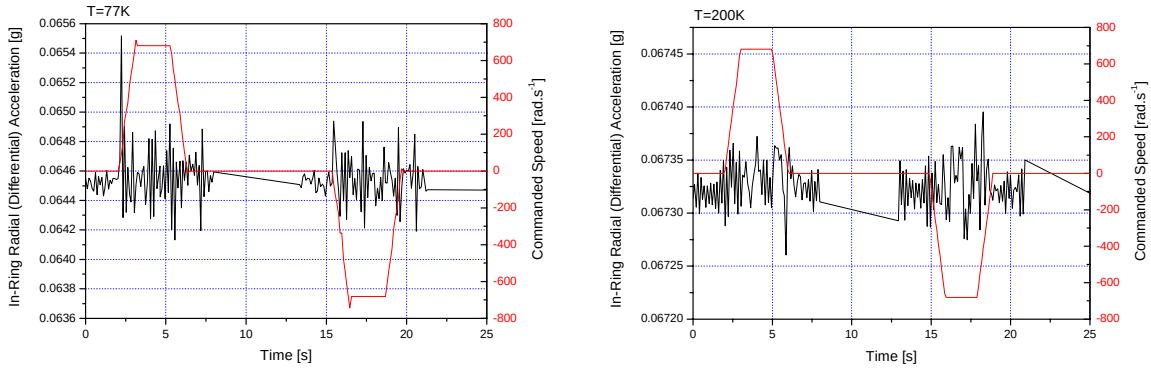

Figure 3.5-2 YBCO In-Ring Radial Differential Sensor Comparison at 77K and 200K

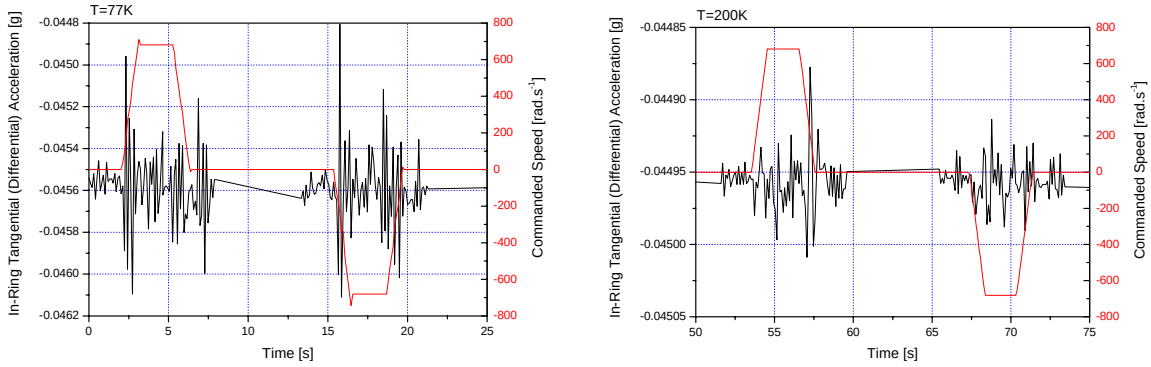

Figure 3.5-3 YBCO In-Ring Tangential Differential Sensor Comparison at 77K and 200K

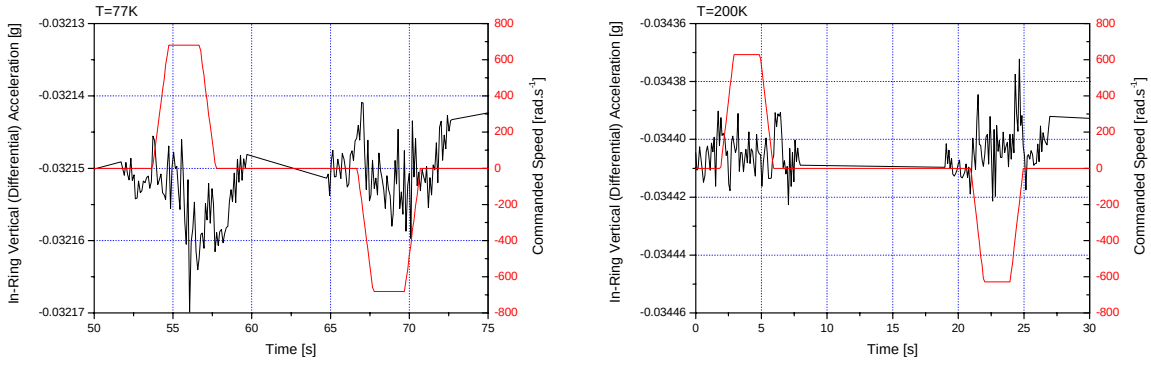

Figure 3.5-4 YBCO In-Ring Vertical Differential Sensor Comparison at 77K and 200K

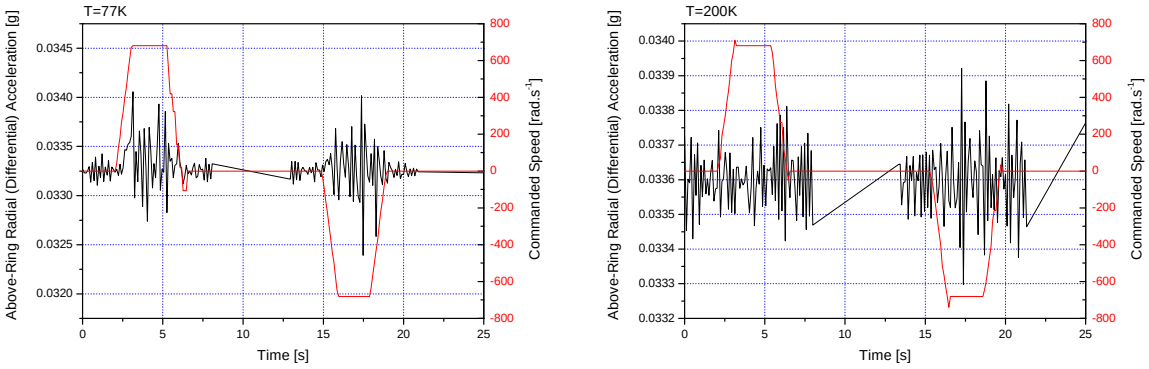

Figure 3.5-5 YBCO Above-Ring Radial Differential Sensor Comparison at 77K and 200K

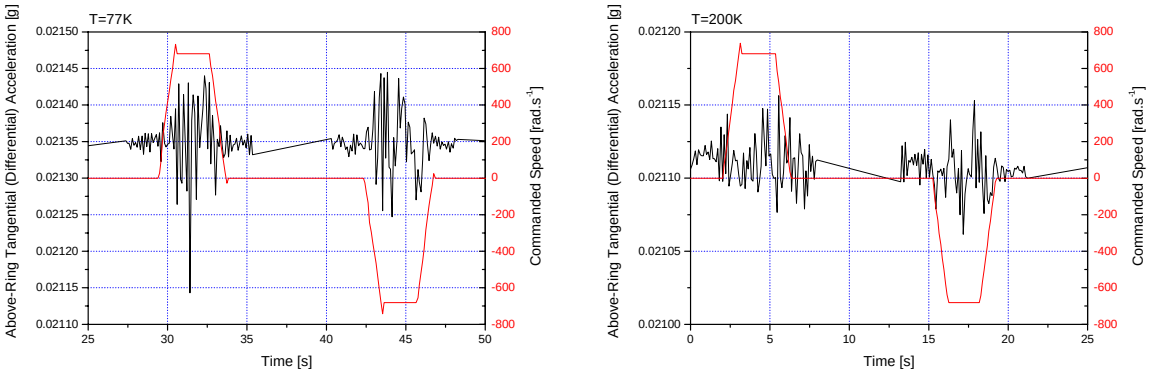

Figure 3.5-6 YBCO Above-Ring Tangential Differential Sensor Comparison at 77K and 200K

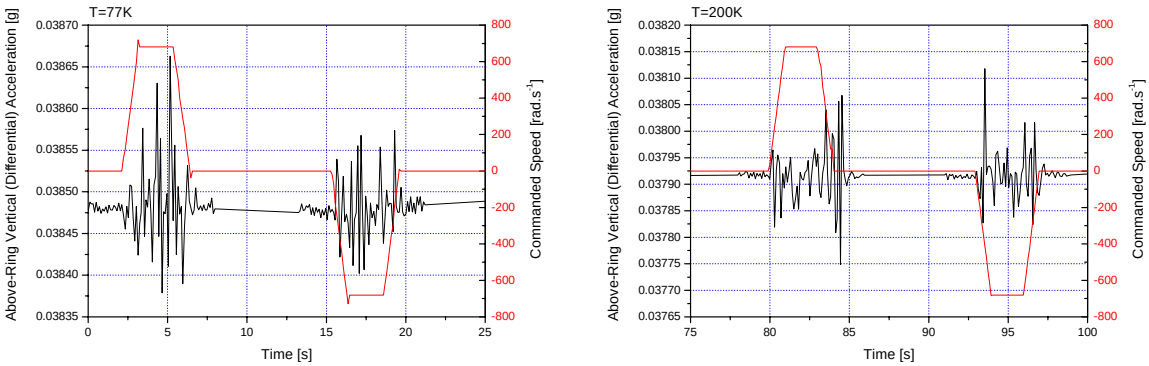

Figure 3.5-7 YBCO Above-Ring Vertical Differential Sensor Comparison at 77K and 200K

	77K				200K			
	Acceleration Coupling Factor		Correlation Factor		Acceleration Coupling Factor		Correlation Factor	
Position	**Mean**	**Sigma**	**Mean**	**Sigma**	**Mean**	**Sigma**	**Mean**	**Sigma**
In-Ring Radial	-7.96E-09	4.16E-08	-0.02	0.20	6.63E-09	8.37E-09	0.07	0.09
In-Ring Tangential	5.66E-09	1.31E-08	0.04	0.07	-5.66E-09	7.53E-09	-0.08	0.11
In-Ring Vertical	-6.17E-10	2.54E-09	-0.07	0.22	2.11E-09	3.42E-09	0.08	0.13
Above-Ring Radial	-8.58E-09	3.21E-08	-0.01	0.04	2.06E-08	1.25E-08	0.05	0.03
Above-Ring Tangential	-2.27E-09	1.12E-08	-0.02	0.09	3.24E-09	3.87E-09	0.06	0.07
Above-Ring Vertical	-4.82E-09	1.44E-08	-0.04	0.11	-1.58E-09	3.58E-08	-0.01	0.22

Table 10 YBCO Acceleration Coupling at 77K and 200K (Over 20 Profiles)

	77K				200K			
	Velocity Coupling Factor		Correlation Factor		Velocity Coupling Factor		Correlation Factor	
Position	**Mean**	**Sigma**	**Mean**	**Sigma**	**Mean**	**Sigma**	**Mean**	**Sigma**
In-Ring Radial	-1.74E-08	6.01E-08	-0.08	0.30	-4.14E-09	2.63E-08	-0.05	0.24
In-Ring Tangential	-2.45E-09	5.45E-08	-0.01	0.25	-8.80E-10	2.14E-08	0.00	0.26
In-Ring Vertical	-4.92E-10	1.33E-08	-0.01	0.44	-2.16E-11	9.64E-09	-0.03	0.30
Above-Ring Radial	8.66E-09	6.92E-08	0.01	0.08	-1.74E-09	3.23E-08	0.00	0.08
Above-Ring Tangential	2.87E-09	1.94E-08	0.03	0.15	1.29E-09	1.33E-08	0.00	0.23
Above-Ring Vertical	-1.44E-09	2.48E-08	-0.01	0.15	2.22E-09	3.47E-08	0.02	0.17

Table 11 YBCO Velocity Coupling at 77K and 200K (Over 20 Profiles)

	77K				200K			
	Velocity^2 Coupling Factor		Correlation Factor		Velocity^2 Coupling Factor		Correlation Factor	
Position	**Mean**	**Sigma**	**Mean**	**Sigma**	**Mean**	**Sigma**	**Mean**	**Sigma**
In-Ring Radial	5.60E-11	7.86E-11	0.17	0.23	3.21E-11	1.46E-11	0.20	0.09
In-Ring Tangential	-5.56E-11	5.64E-11	-0.17	0.15	-2.55E-11	1.51E-11	-0.21	0.12
In-Ring Vertical	-1.71E-11	1.33E-11	-0.36	0.25	-1.36E-11	5.54E-12	-0.28	0.11
Above-Ring Radial	8.84E-11	4.26E-11	0.07	0.03	3.86E-11	1.41E-11	0.06	0.02
Above-Ring Tangential	-3.40E-12	3.22E-11	-0.01	0.16	1.65E-11	7.10E-12	0.19	0.08
Above-Ring Vertical	-2.28E-11	3.20E-11	-0.09	0.12	-4.11E-11	2.95E-11	-0.14	0.09

Table 12 YBCO Velocity^2 Coupling at 77K and 200K (Over 20 Profiles)

4 DISCUSSION

The facility reached the design specification of Phase I and can reliably detect gravitational anomalies in rotating superconductors that are low enough to test our theory that non-classical gravitational fields are responsible for the Tate Cooper-pair mass anomaly – the design goal of Phase I. Coupling factors for all sensor directions (radial, tangential and vertical - inside and above the superconductor) were evaluated for applied angular acceleration, angular speed and angular speed^2 (applied centrifugal acceleration).

It could be shown that the liquid nitrogen level and external magnetic fields (e.g. from the electric motor) have no influence on the measurement and that the sensors are sufficient mechanically de-coupled to reach very low signal levels even during maximum accelerations. Both speed and accelerations obtained exceed the specifications of Phase I.

Both BSCCO and YBCO measurements showed coupling factor values similar to the dummy test with Niobium at liquid nitrogen temperatures (77 K). In addition, no significant difference between measurements at 77 K and room temperatures were seen. Nearly all mean values (expect some very low numbers at ω^2 coupling factor measurements) are below the sigma values. Therefore, the sigma values can be interpreted as upper limits for a possible coupling factor between applied acceleration/speed to a superconductor and induced gravitational fields.

Table 13 compares the upper limits for the angular acceleration coupling factor (our primary theoretical prediction) in the tangential direction with the values originally derived from Tate's experiment and our latest theoretical values.

Material	Condition	Predicted Angular Acceleration Coupling Factor [$s^2.rad^{-1}$]	Measured Upper Limit Angular Acceleration Coupling Factor [$s^2.rad^{-1}$]
Niobium @ 6 K	From Tate's Experiment	-3.7×10^{-7}	NA
Niobium @ 6 K	From Theory	-1.2×10^{-8}	NA
YBCO @ 77 K	From Theory	-6.1×10^{-10}	$\pm 1.3 \times 10^{-8}$
BSCCO (2212) @ 77 K	From Theory	-2.6×10^{-10}	$\pm 4.8 \times 10^{-9}$

Table 13 Comparison of Measured Upper Limits on Angular Acceleration Couplings with Theoretical Precitions Inside Superconductor Ring in Tangential Direction

This shows that the resolution of the facility is one order of magnitude above the theoretical predictions for YBCO and BSCCO, but it is accurate enough to test induced gravitational fields for Tate's condition of using Niobium. The tests also rule out gravitational fields as large as predicted from Tate's measurements to exist for YBCO and BSCCO high-temperature superconductors.

The resolution of the AppliedMEMS sensors (≅ 1 μg) have not been reached yet, an improvement of about one order of magnitude should be still possible. It was found out that the largest noise contribution is due to the acoustic noise developed by the bottom bearing. Alternative bearing solutions such a frictionless magnetic bearing or a distribution of the bearing loads to several bearings could improve the noise level.

From the latest theoretical work it seems also more worthwhile to continue the experiments with low-temperature superconductors and liquid helium, as the facility resolution to detect gravitational anomalies e.g. for Niobium is already reached, and much larger gravitational fields can be expected.

5 CONCLUSIONS

The following conclusions have been obtained during Phase II of this project:

- A facility was designed and built to investigate μg level gravitational fields around rotating superconductors exceeding the specifications of Phase I. Angular acceleration coupling factor resolutions around $1x10^{-8}$ $s^{-2}.rad^{-1}$ were obtained.

- The coupling factors are small enough to test the originally predicted gravitational fields based on Tate's Cooper-pair measurement (about 10^{-7} $s^{-2}.rad^{-1}$).

- No gravitational anomalies have been detected using BSCCO and YBCO high-temperature superconductors, as expected from latest theoretical work (at least one order of magnitude below the facilities resolution, around $1x10^{-9}$ $s^{-2}.rad^{-1}$).

- The resolution can be further increased by reducing the acoustic noise coming from the bottom bearing (exposed to cryogenic temperatures) by using either frictionless magnetic bearings or optimizing the current bearing solution (e.g. by dividing the bearing load to several bearings).

- The most promising venue seems to explore low-temperature superconductors such as Niobium at liquid helium temperatures to definitely test under the same condition as Tate did for her Cooper-pair measurement. Due to the much higher Cooper-pair density, larger gravitational fields should be produced as theoretically predicted.

REFERENCES

de Matos, C.J., and Tajmar, M., "Gravitomagnetic London Moment and the Graviton Mass Inside a Superconductor", *Physica C*, in Print (2005)

Capelle, K., and Gross, E.K.U., "Relativistic framework for microscopic theories of superconductivity. I. The Dirac equation for superconductors", *Physical Review B*, Vol. 59, 1999, pp. 7140-7154

Modanese, G., "Local Contribution of a Quantum Condensate to the Vacuum Energy Density", *Mod. Phys. Lett. A*, 18(10), 2003, pp. 683-690

Novello, M., and Neves, R.P., "The Mass of the Graviton and the Cosmological Constant", *Classical and Quantum Gravity*, 20, 2003, L67-L73

Ryder, L.H., "Quantum Field Theory", Cambridge University Press, 2nd Edition, 1996, pp. 296-298

Tajmar, M., and de Matos, C.J., "Gravitomagnetic Field of a Rotating Superconductor and of a Rotating Superfluid", *Physica C*, Vol. 385, No. 4, 2003, pp. 551-554

Tajmar, M., and de Matos, C.J., "Extended Analysis of Gravitomagnetic Fields in Rotating Superconductors and Superfluids", *Physica C*, Vol. 420, No. 1-2, 2005, pp. 56-60

Tate, J., Cabrera, B., Felch, S.B., Anderson, J.T., "Precise Determination of the Cooper-Pair Mass", *Physical Review Letters*, 62(8), 1989, pp 845-848

Tate, J., Cabrera, B., Felch, S.B., Anderson, J.T., "Determination of the Cooper-Pair Mass in Niobium", *Physical Review B*, 42(13), 1990, pp 7885-7893

DISTRIBUTION LIST

AFRL-MN-EG-TR-2007-7013

Defense Technical Info. Center 1
8725 John J. Kingman Rd Ste 0944
Fort Belvoir VA 22060-6218

Eglin AFB offices:

AFRL/MNOC-1 (STINFO Office)	1
AFRL/MN CA-N	1
AFRL/MNME	1
AFRL/MNMF	1
AFRL/MNMW	1
AFRL/MNMI	1